Supporting Information

Evidence of aggregation-assisted antibacterial photodynamic activity against S. aureus and E. coli using amphiphilic Ru(II) polypyridyl complexes

Athanasios K. Sakellariou,[a] Sofia Alexandra Tsoni,[a] Despoina Varna,[a] Maria Nikopoulou,[b] Eleni Pavlidou,[c] Rigini Papi,[a] Sylvestre Bonnet,[d] and Theodore Lazarides[a,*]

[a] *Department of Chemistry, Aristotle University of Thessaloniki, 54124 Thessaloniki, Greece, tlazarides@chem.auth.gr.*

[b] *Department of Geology, Aristotle University of Thessaloniki, 54124 Thessaloniki, Greece.*

[c] *Department of Physics, Aristotle University of Thessaloniki, 54124 Thessaloniki, Greece.*

[d] *Leiden Institute of Chemistry, Leiden University, Einsteinweg 55, 2333CC Leiden, The Netherlands.*

Table of Contents

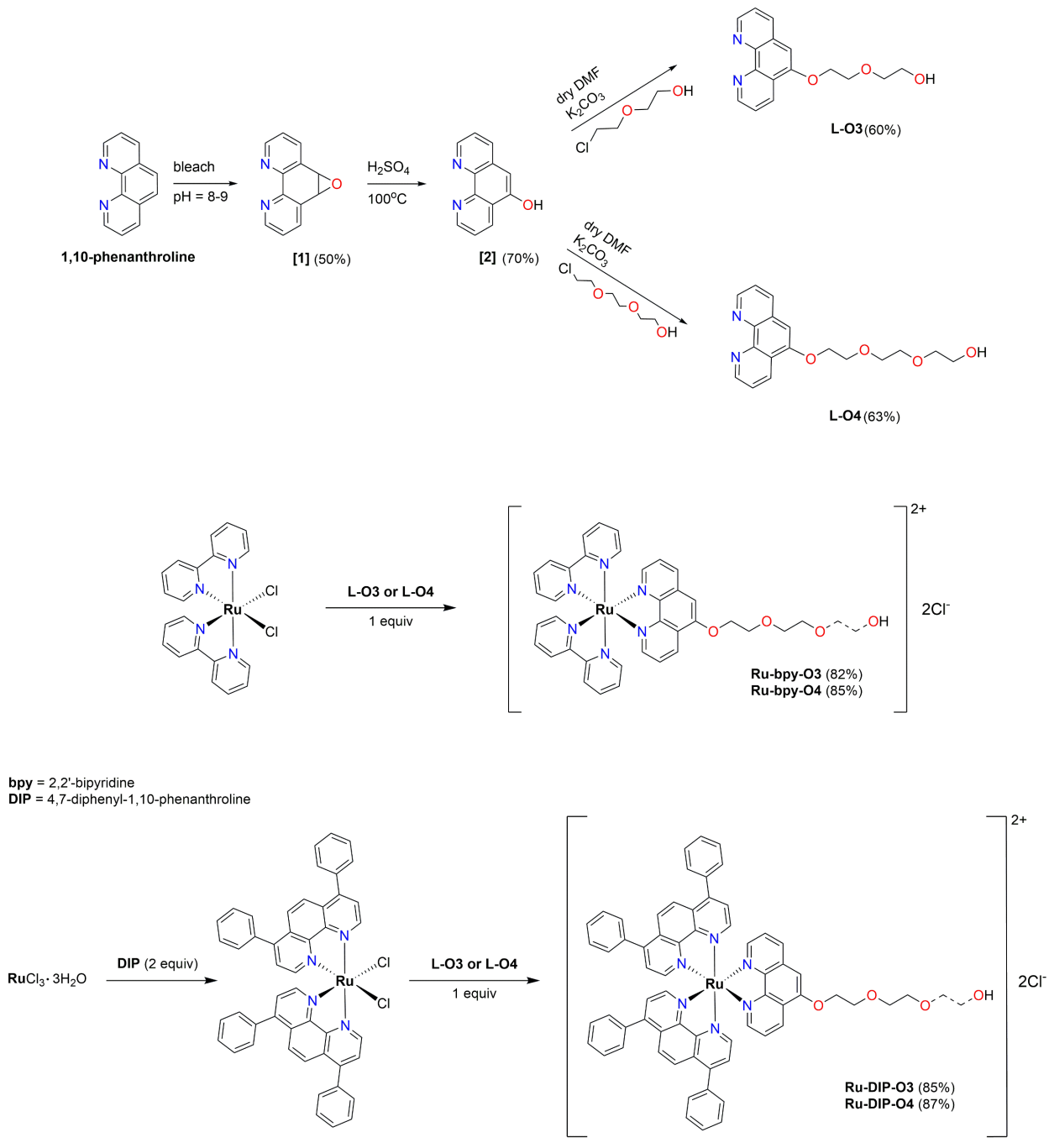

Figure S1 *General synthetic route.*

Ligand characterisation (NMR, ESI-MS)

The ^{1}H-NMR spectra of **L-O3** and **L-O4** are shown in Figures S2 and S3, together with the proton numbering schemes and peak assignments. The assignments were performed by comparison with the ^{1}H-NMR spectra of the precursor compounds 1,10-phenanthroline-5,6-oxide **[1]** and 5-hydroxy-1,10-phenanthroline **[2]** (Figures S6–S7), as well as on the basis of the expected chemical shifts and coupling patterns of substituted phenanthroline derivatives. The singlet at δ 7.65 ppm is attributed to the uncoupled phenanthroline proton d. The remaining aromatic protons appear as three sets of closely related signals: g/a (δ 9.20 and 9.02 ppm), e/c (δ 8.70 and 8.10 ppm) and f/b (δ 7.65 and 7.56 ppm). The most downfield pair (g/a) is assigned to the protons adjacent to the nitrogen atoms, consistent with their increased deshielding. The f/b pair appears as doublets of doublets, as expected for protons coupled to two non-equivalent neighbours, while the e/c pair corresponds to the remaining aromatic doublets. The coupling constants further support these assignments: protons g, e and f (J = 4.3, 8.2 and 8.2/4.3 Hz, respectively) form one spin system, while a, c and b (J = 4.2, 8.1 and 8.1/4.2 Hz, respectively) form the second. The g/e/f set is attributed to the pyridine ring closer to the substitution site, as these protons are consistently shifted downfield relative to their counterparts (a/c/b), in agreement with the electron-withdrawing influence of the oxygen substituent. This trend is consistent with literature reports for oxygen-substituted phenanthroline derivatives.[1] Integration of the ^{1}H-NMR spectra is consistent with the expected number of protons in both the aromatic and aliphatic regions. The polyether chain displays the characteristic triplet patterns corresponding to the -CH_2- groups. Further proof of structure is given by the expected m/z values shown in Figures S4 and S5 where $[M]^+$ and $[2M+Na]^+$ species are detected for both ligands.

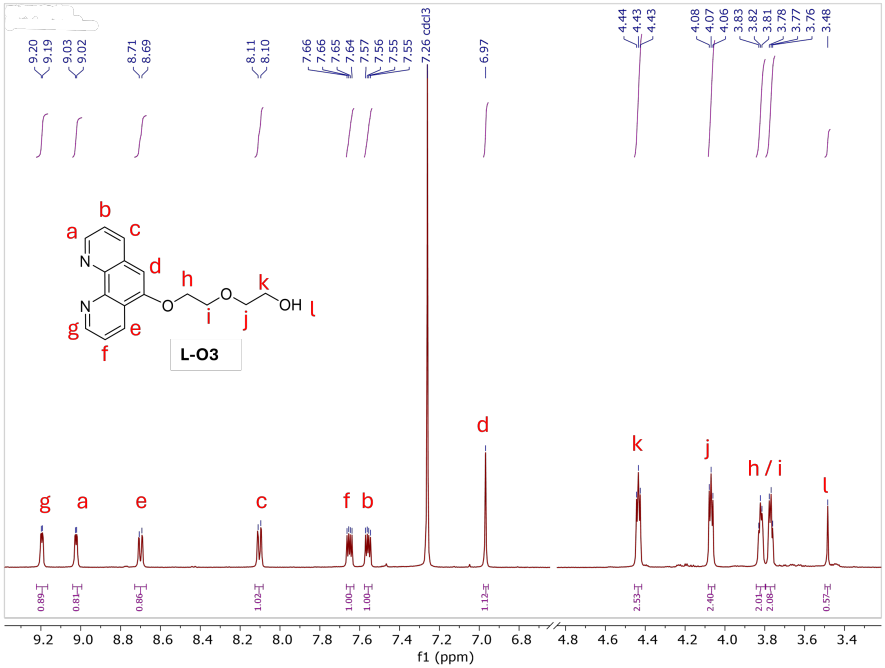

Figure S2 *Assigned ^{1}H-NMR spectrum of* ***L-O3*** *in $CDCl_3$.*

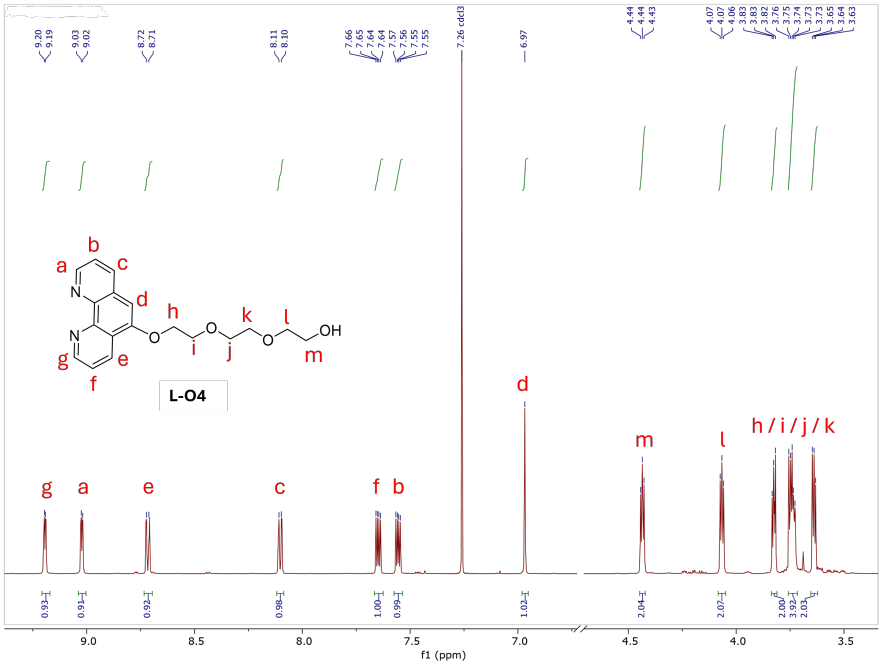

Figure S3 *Assigned ^{1}H-NMR spectrum of* ***L-O4*** *in $CDCl_3$.*

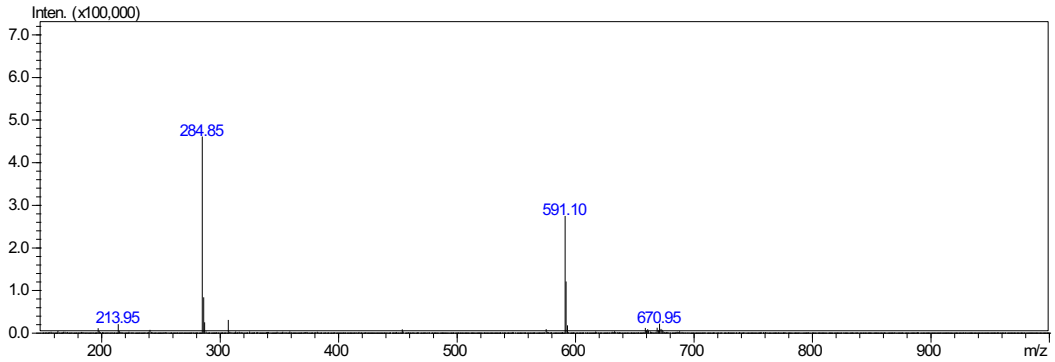

Figure S4 *ESI-MS spectrum of* ***L-O3*** *(positive detection mode). Theoretical calculation for $[M+H]^+$ = 285.12 and for $[2M+Na]^+$ = 591.22 - experimental value s = 284.85 and 591.10 respectively.*

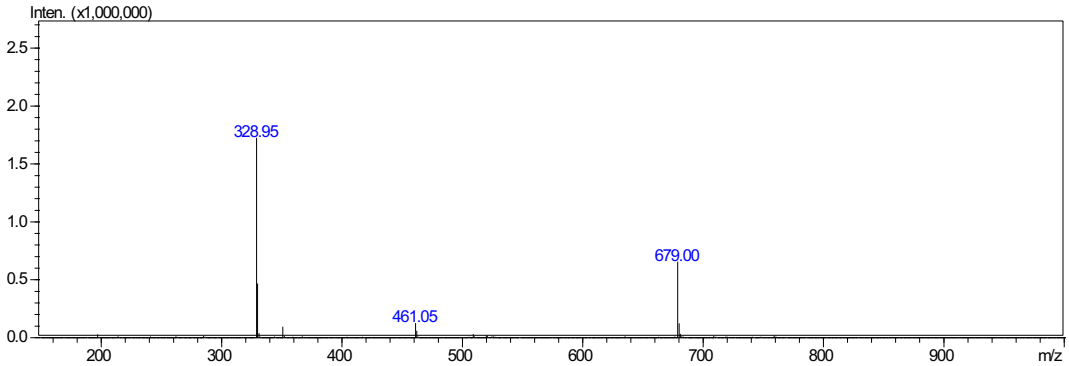

Figure S5 *ESI-MS spectrum of* ***L-O4*** *(positive detection mode). Theoretical calculation for $[M+H]^+$ = 329.14 and for $[2M+Na]^+$ = 679.26 – experimental value = 328.95 and 679.00 respectively.*

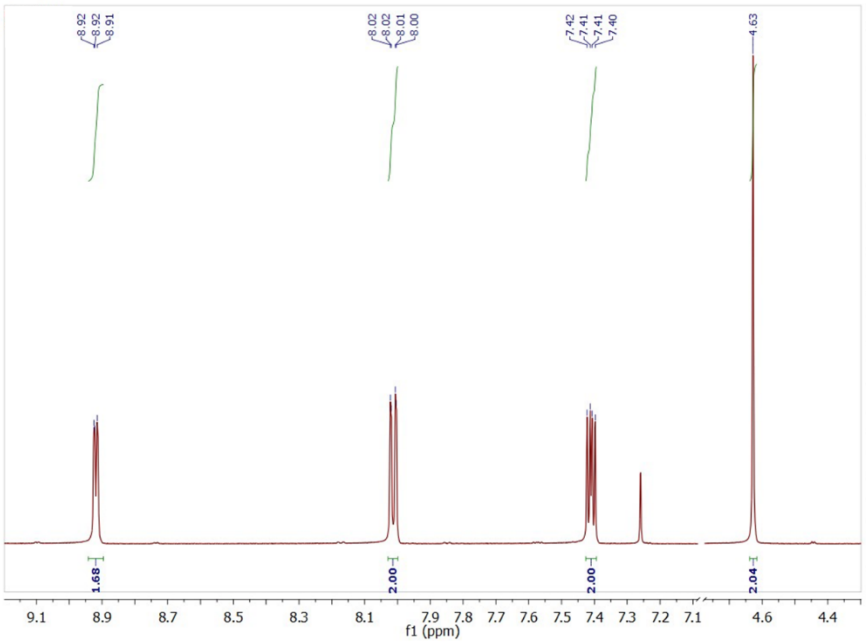

Figure S6 *^{1}H-NMR spectrum of 1,10-Phenanthroline-5,6-oxide* ***[1]*** *in $CDCl_3$.*

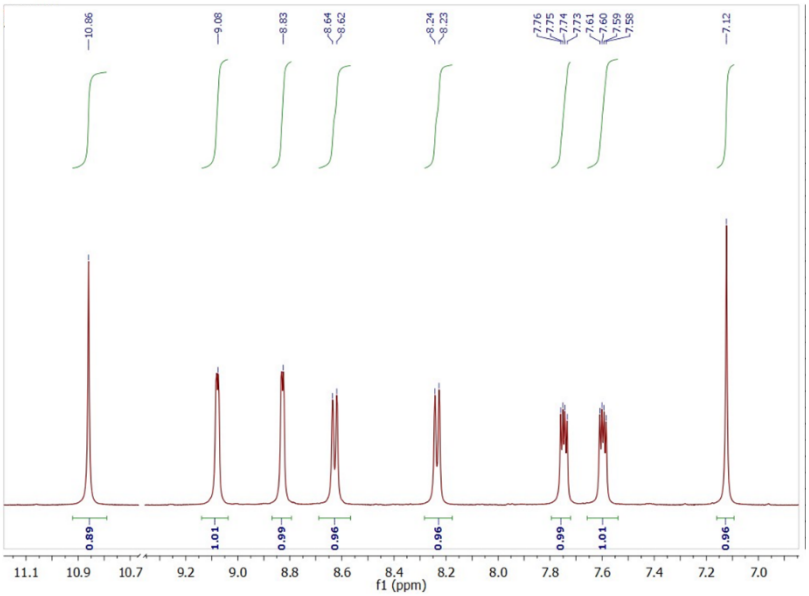

Figure S7 *^{1}H-NMR spectrum of 5-hydroxy-1,10-phenanthroline* ***[2]*** *in DMSO-d_6.*

1 W. Paw and R. Eisenberg, Synthesis, Characterization, and Spectroscopy of Dipyridocatecholate Complexes of Platinum, *Inorg. Chem.*, 1997, **36**, 2287–2293.

Complexes characterisation (NMR, HRMS, LC-MS)

The ^{1}H-NMR spectra of compounds **Ru-bpy-O3** and **Ru-bpy-O4** can be seen in Figures S8, S9 and S13, together with proton numbering schemes and peak assignments based on the ^{1}H-^{1}H COSY spectra. Protons associated with the bpy ancillary ligands are denoted by the subscript "b", while those corresponding to the **L-O3** or **L-O4** phenanthroline ligands are denoted by the subscript "p". The peaks corresponding to the protons of the bpy ligands are split into two sets as the two halves of each bpy ligand are inequivalent. The bpy protons $1_b/1'_b$, which are brought to close contact due to complexation, give rise to two sets of closely spaced doublets at δ ca. 8.72 ppm while the two doublets at 8.53 and 8.94 ppm are attributed to the phenanthroline protons adjacent to the nitrogen atoms 1_p and 7_p. The peaks corresponding to the bpy protons adjacent to the nitrogen atoms $4_b/4'_b$ can be seen at ca. 7.62 and 7.92 ppm showing the expected upfield shift in comparison to free bpy due to the shielding effects induced by the ring currents of the adjacent ligands. The assignment of the rest of the bpy and phen protons follows naturally by examination of the two-dimensional correlation experiments (COSY/HSQC), which show the expected proton-proton and proton-carbon connectivities, as well as by comparison with the **L-O3** and **L-O4** ^{1}H-NMR spectra (Figures S2-3) which provide an easily recognizable pattern for the phen protons. The singlet peak observed at 7.65 ppm is attributed to the uncoupled phenanthroline proton 4_p. The ^{1}H-NMR spectra of **Ru-DIP-O3** and **Ru-DIP-O4** were assigned analogously. However, the large number of aromatic protons and the extensive overlap observed for the peaks of the protons of the phenyl groups prevent full signal assignment. In all cases, high-resolution mass spectrometry shows m/z values in excellent agreement with the simulated isotopic distributions for the respective complexes, while LC-MS confirms composition and purity.

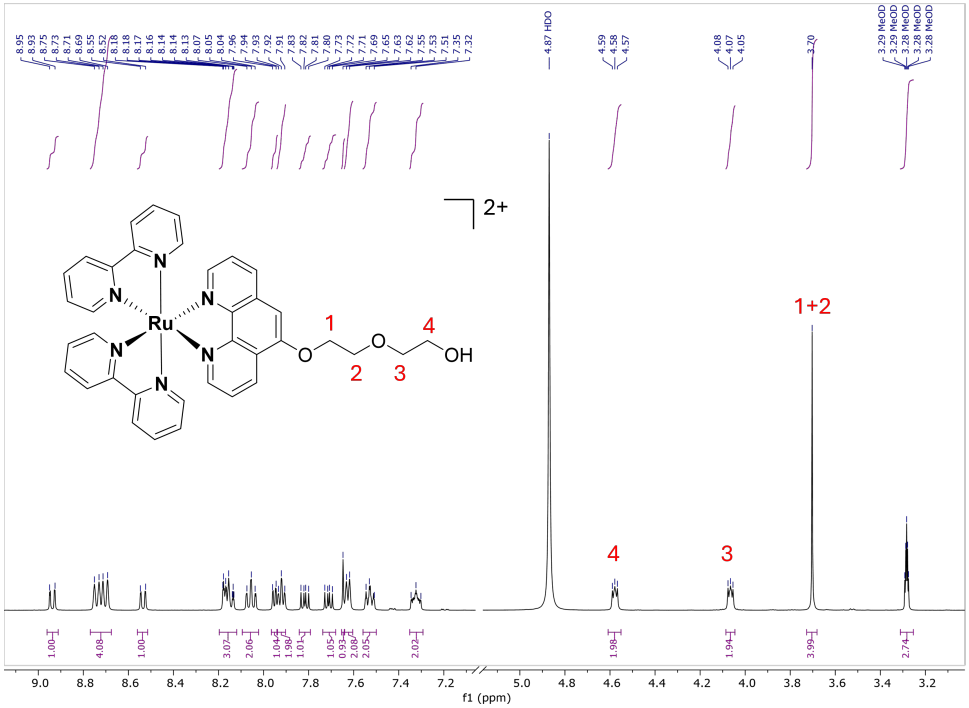

Figure S8 *^{1}H-NMR spectrum of* ***Ru-bpy-O3*** *(total) in CD_3OD.*

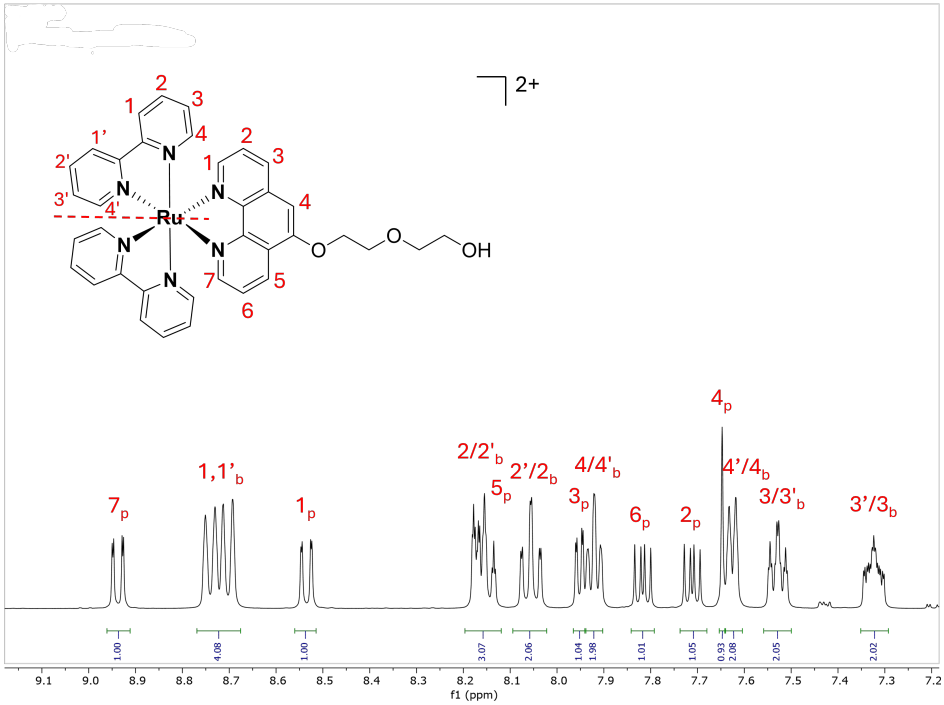

Figure S9 *Assigned ^{1}H-NMR spectrum of* ***Ru-bpy-O3*** *(aromatic region) in CD_3OD.*

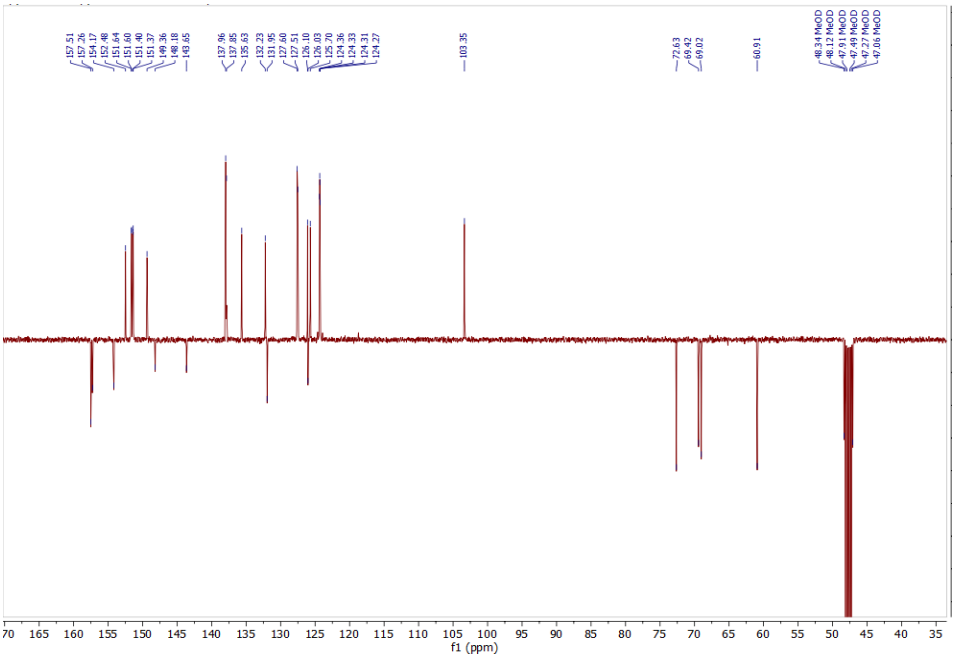

Figure S10 *^{13}C-NMR APT spectrum of* ***Ru-bpy-O3*** *in CD_3OD.*

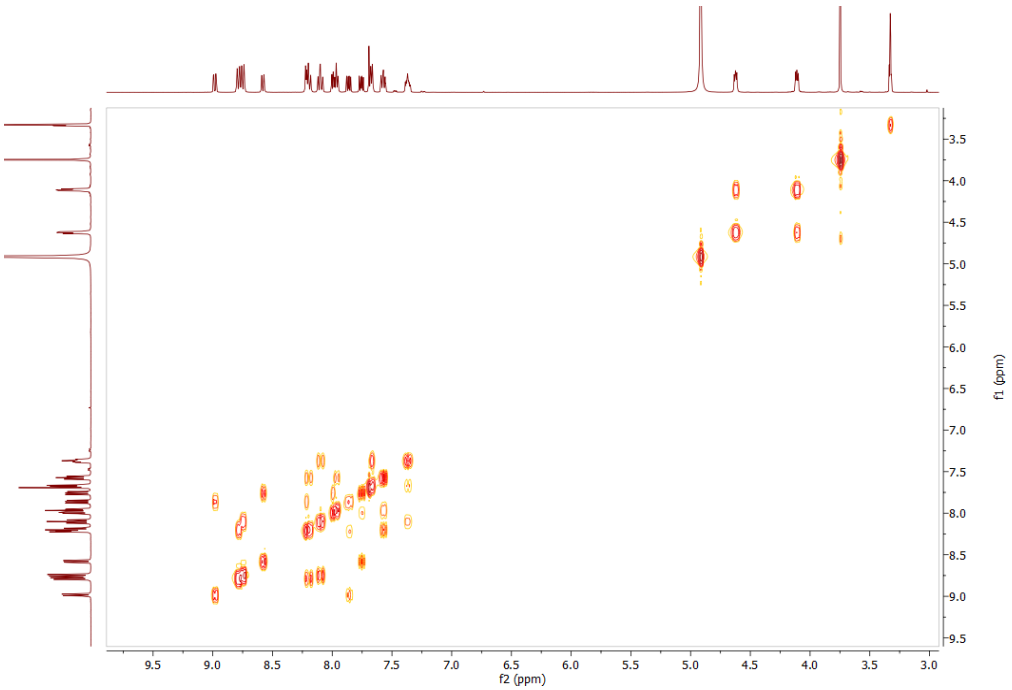

Figure S11 *^{1}H-^{1}H COSY NMR spectrum of* ***Ru-bpy-O3*** *in CD_3OD.*

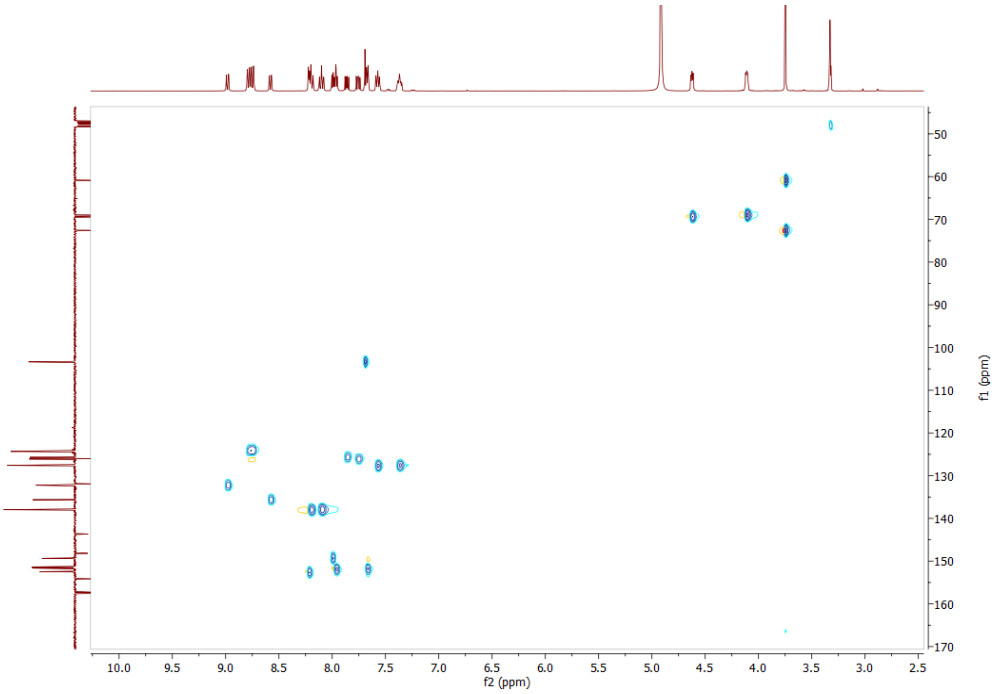

Figure S12 *^{1}H-^{13}C NMR HSQC spectrum of* ***Ru-bpy-O3*** *in CD_3OD.*

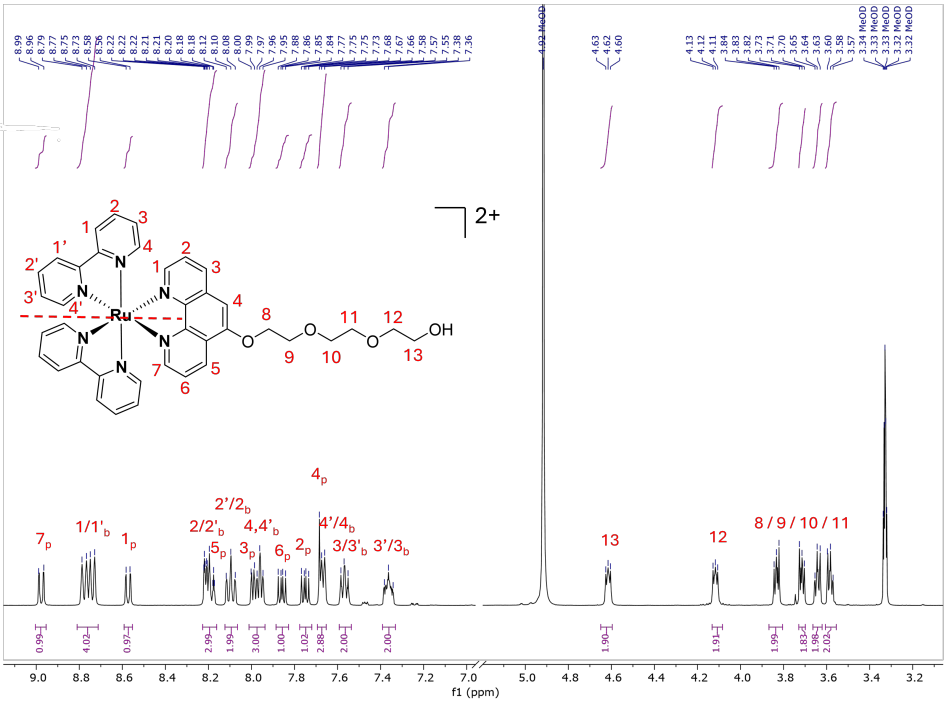

Figure S13 *Assigned ^{1}H-NMR spectrum of* ***Ru-bpy-O4*** *(total) in CD_3OD.*

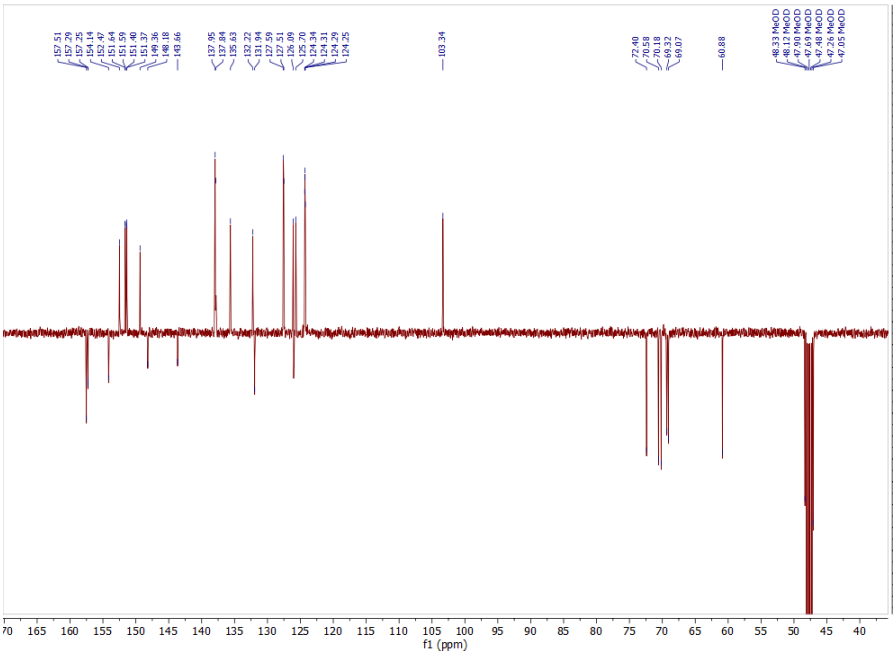

Figure S14 *^{13}C-NMR APT spectrum of* ***Ru-bpy-O4*** *in CD_3OD.*

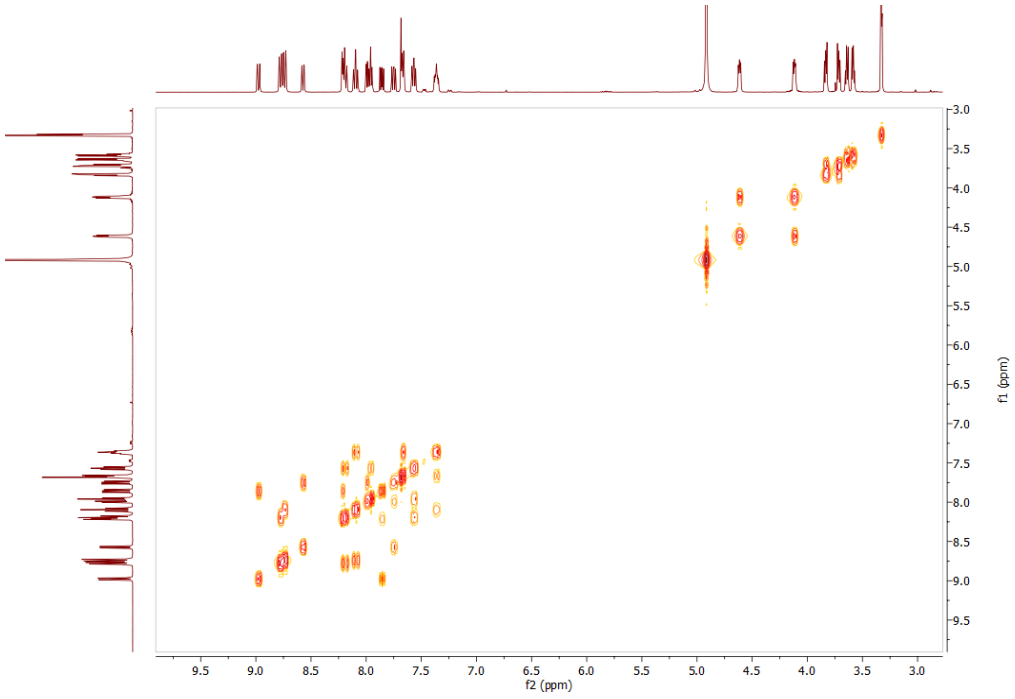

Figure S15 *^{1}H-^{1}H COSY NMR spectrum of* ***Ru-bpy-O4*** *in CD_3OD.*

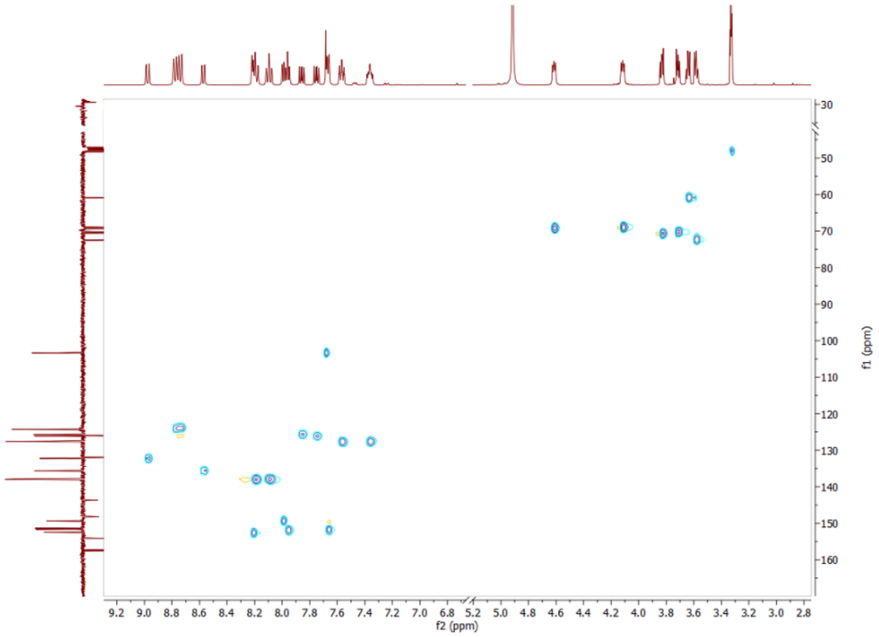

Figure S16 *^{1}H-^{13}C HSQC NMR spectrum of* ***Ru-bpy-O4*** *in CD_3OD.*

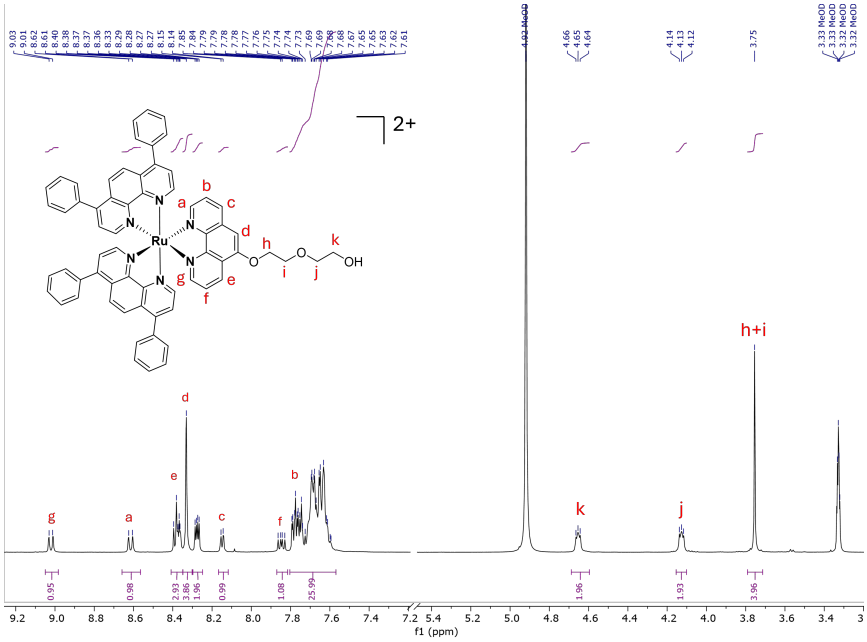

Figure S17 *Assigned ^{1}H-NMR spectrum of* ***Ru-DIP-O3*** *(total) in CD_3OD.*

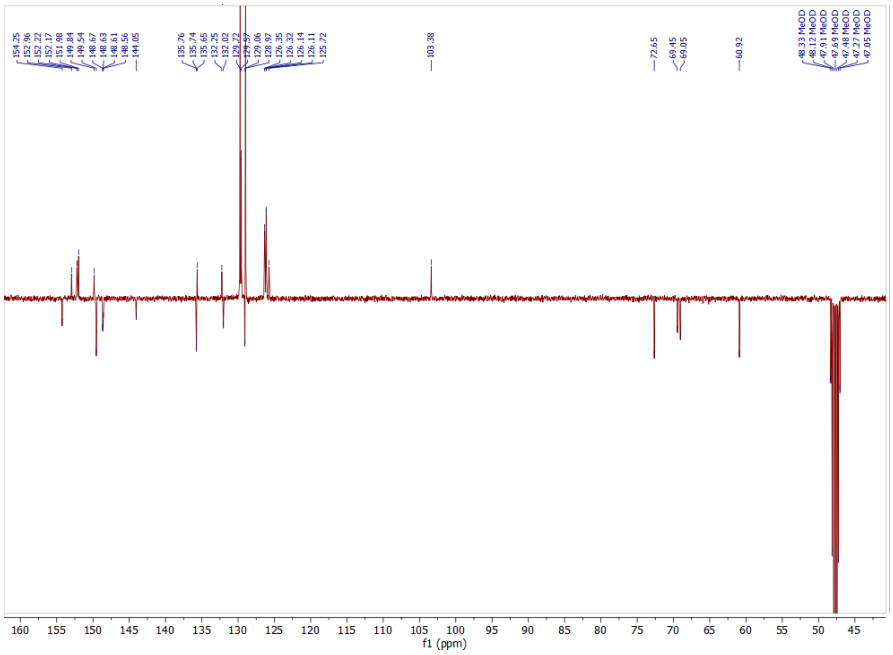

Figure S18 *^{13}C-NMR APT spectrum of* ***Ru-DIP-O3*** *in CD_3OD.*

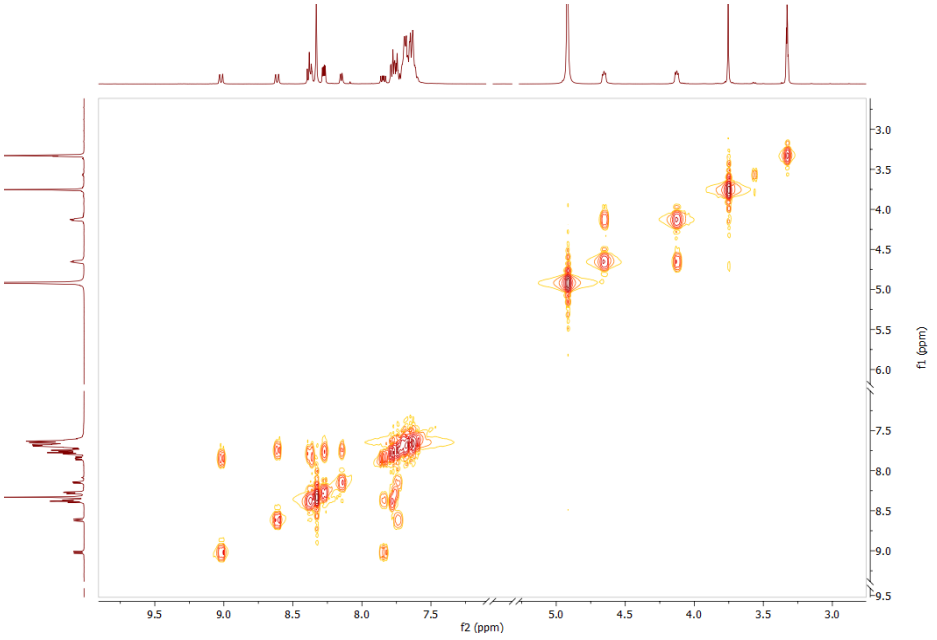

Figure S19 *^{1}H-^{1}H COSY NMR spectrum of* ***Ru-DIP-O3*** *in CD_3OD.*

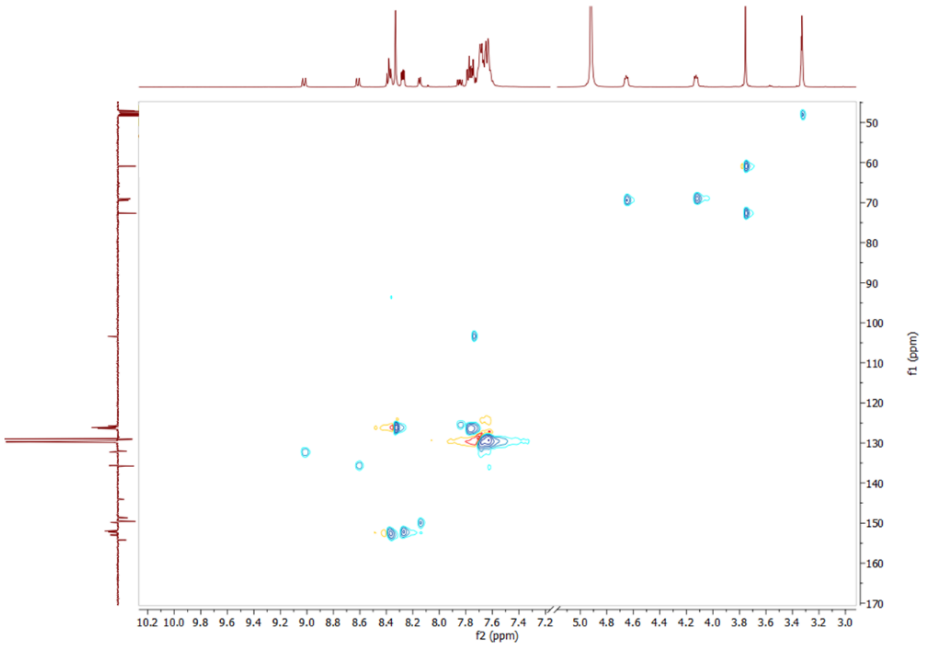

Figure S20 *^{1}H-^{13}C HSQC NMR spectrum of* ***Ru-DIP-O3*** *in CD_3OD.*

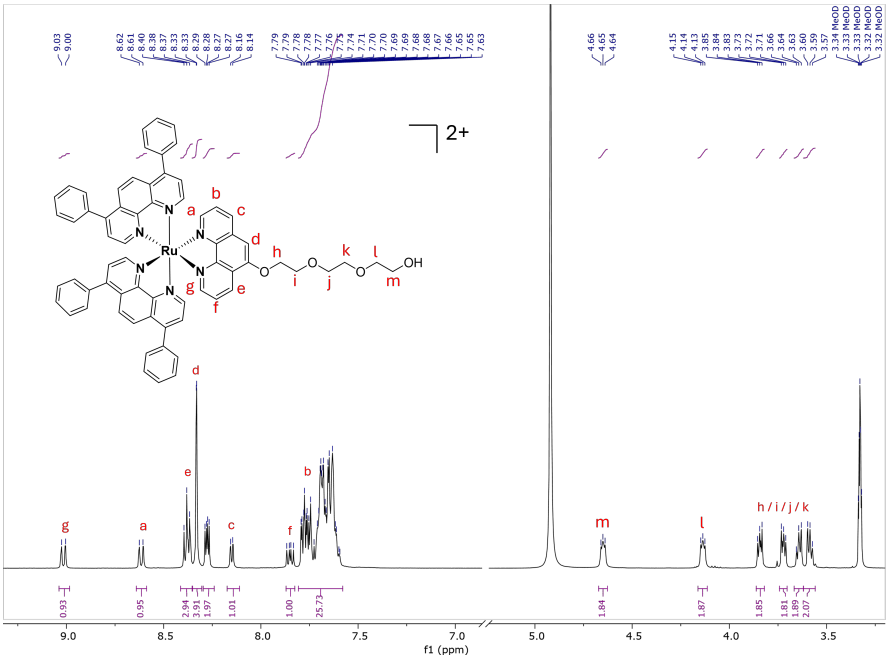

Figure S21 *Assigned ^{1}H-NMR spectrum of* ***Ru-DIP-O4*** *(total) in CD_3OD.*

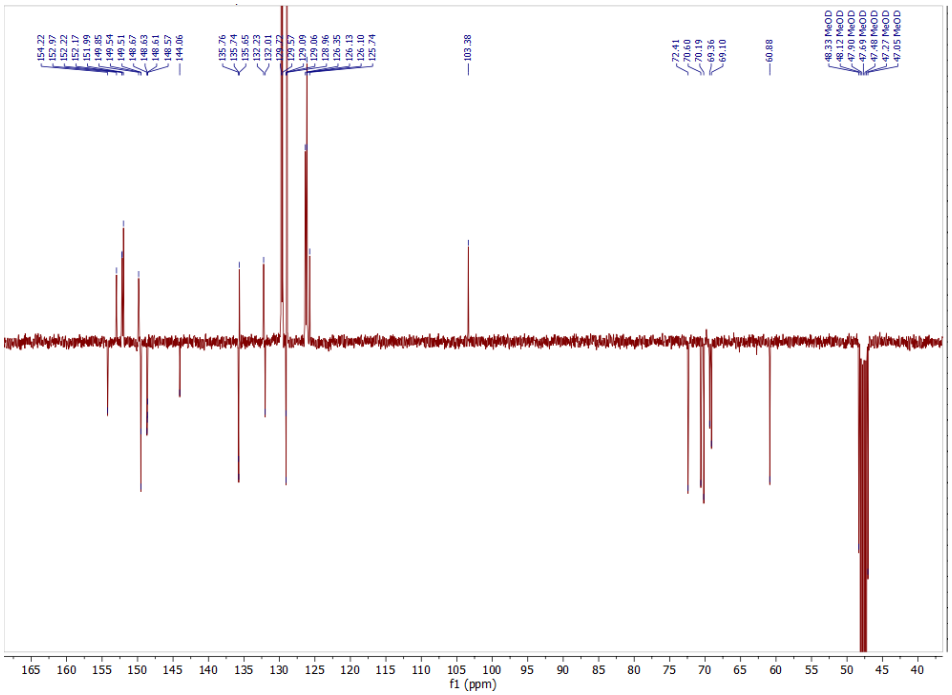

Figure S22 *^{13}C-NMR APT spectrum of* ***Ru-DIP-O4*** *in CD_3OD.*

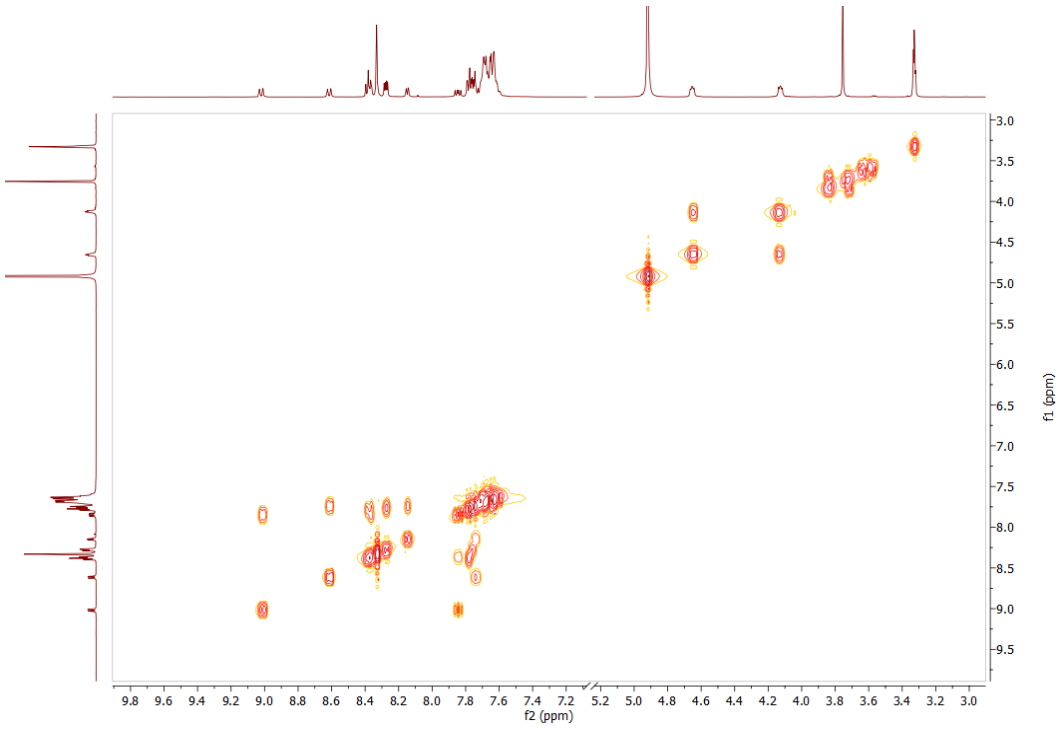

Figure S23 *^{1}H-^{1}H COSY NMR spectrum of* ***Ru-DIP-O4*** *in CD_3OD.*

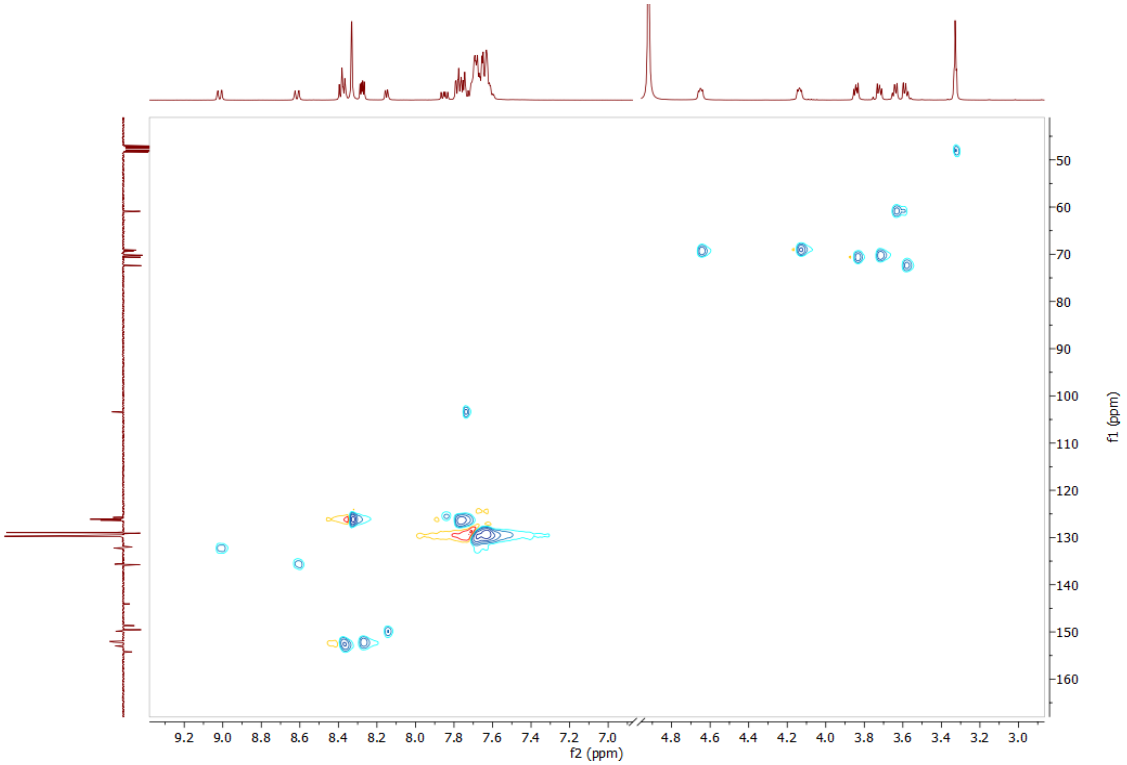

Figure S24 *^{1}H-^{13}C HSQC NMR spectrum of* ***Ru-DIP-O4*** *in CD_3OD.*

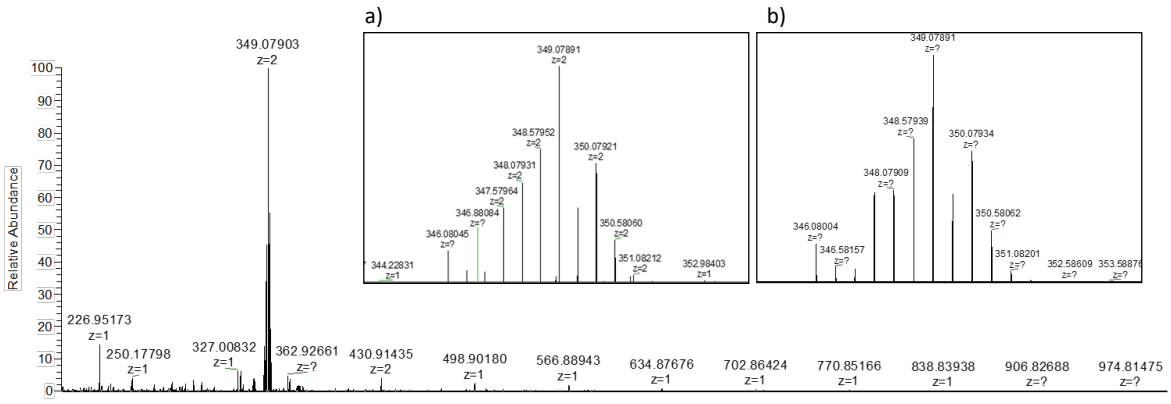

Figure S25 *HRMS spectrum of* ***Ru-bpy-O3****. Inset: a) experimental isotopic distribution b) simulated isotopic distribution.*

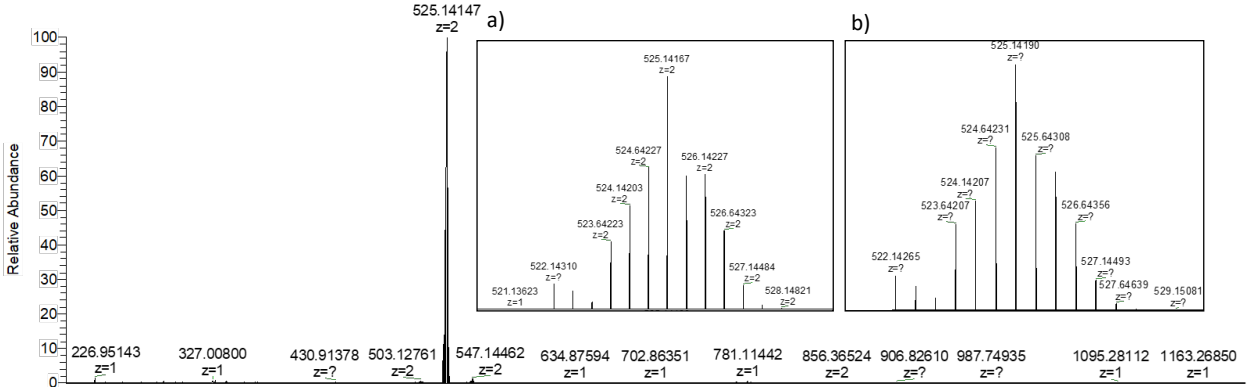

Figure S26 *HRMS spectrum of* ***Ru-DIP-O3****. Inset: a) experimental isotopic distribution b) simulated isotopic distribution.*

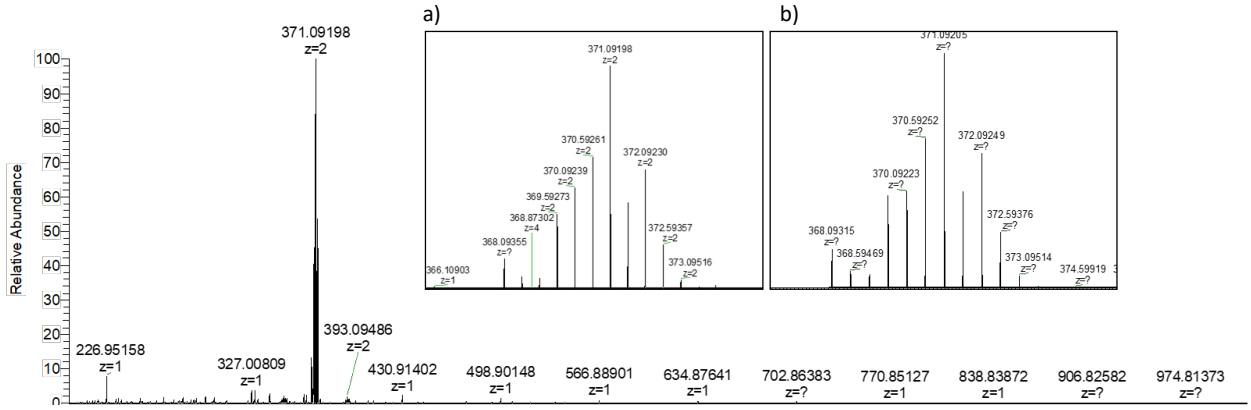

Figure S27 *HRMS spectrum of* ***Ru-bpy-O4****. Inset: a) experimental isotopic distribution b) simulated isotopic distribution.*

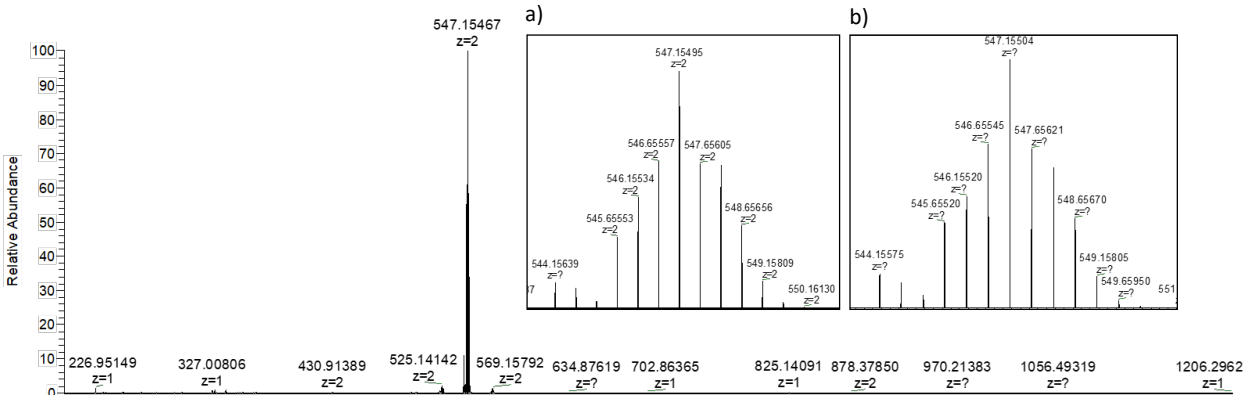

Figure S28 *HRMS spectrum of* ***Ru-DIP-O4****. Inset: a) experimental isotopic distribution b) simulated isotopic distribution.*

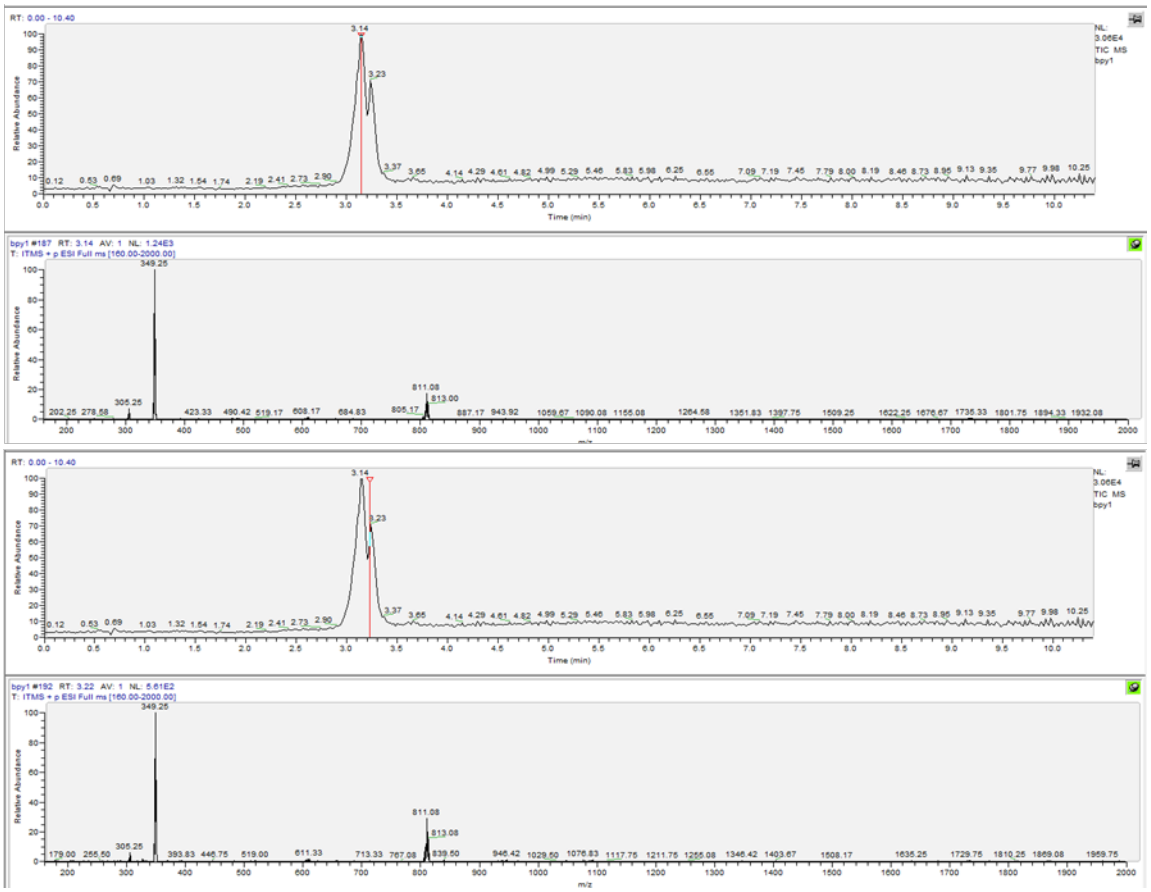

Figure S29 *LC-MS chromatogram of* ***Ru-bpy-O3****.*

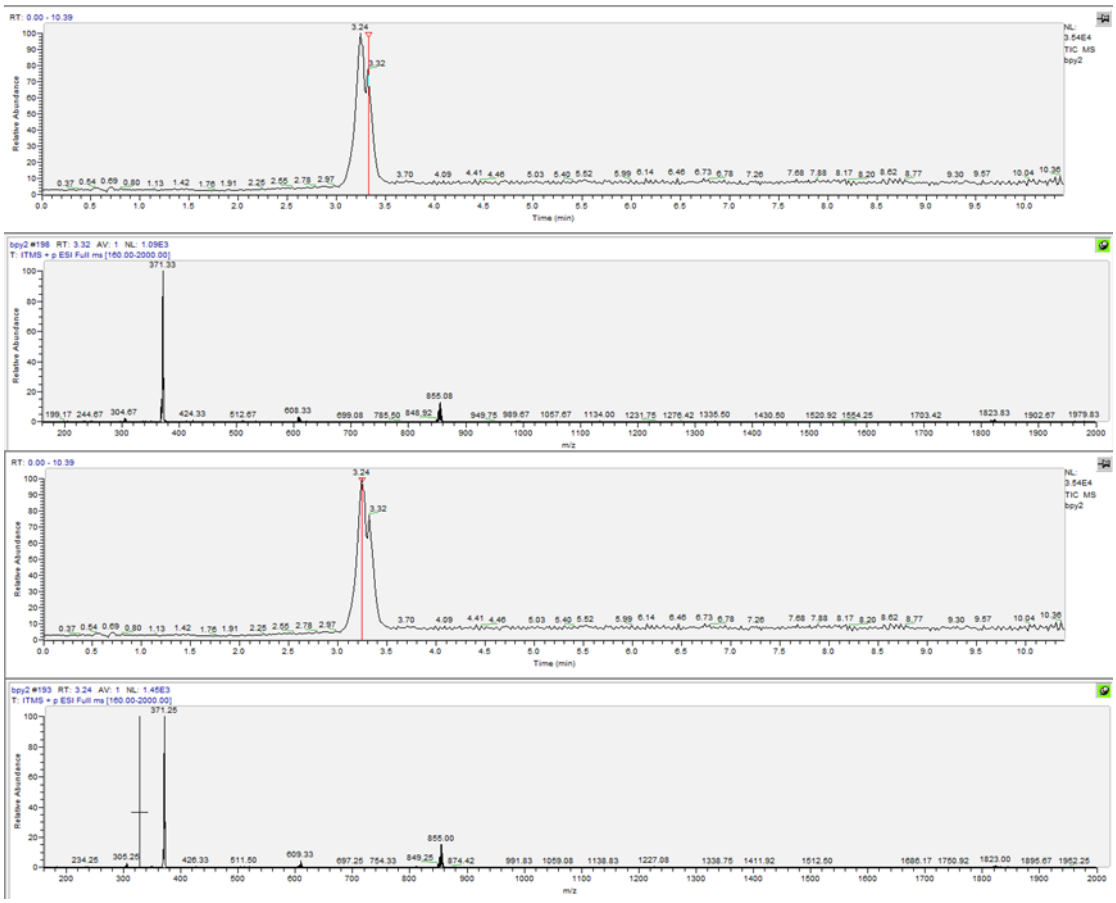

Figure S30 *LC-MS chromatogram of* ***Ru-bpy-O4****.*

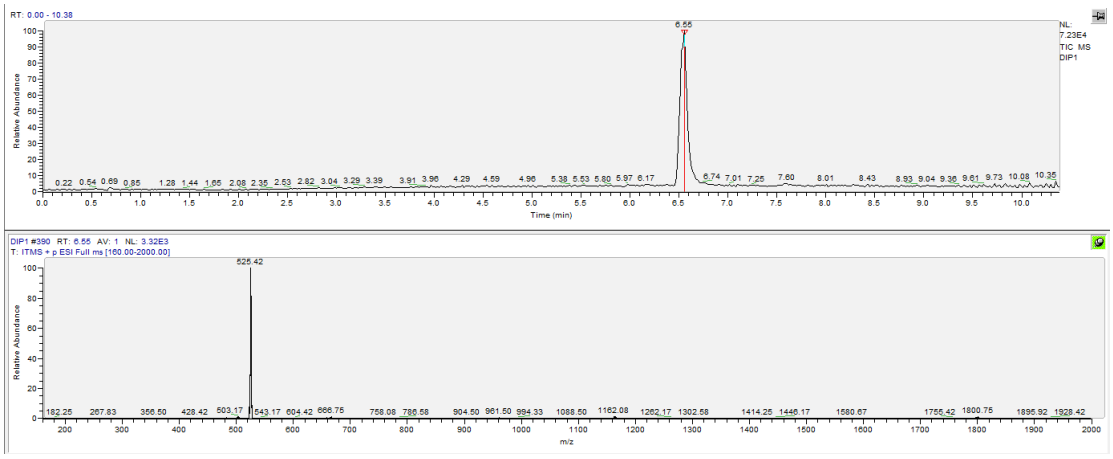

Figure S31 *LC-MS chromatogram of* ***Ru-DIP-O3****.*

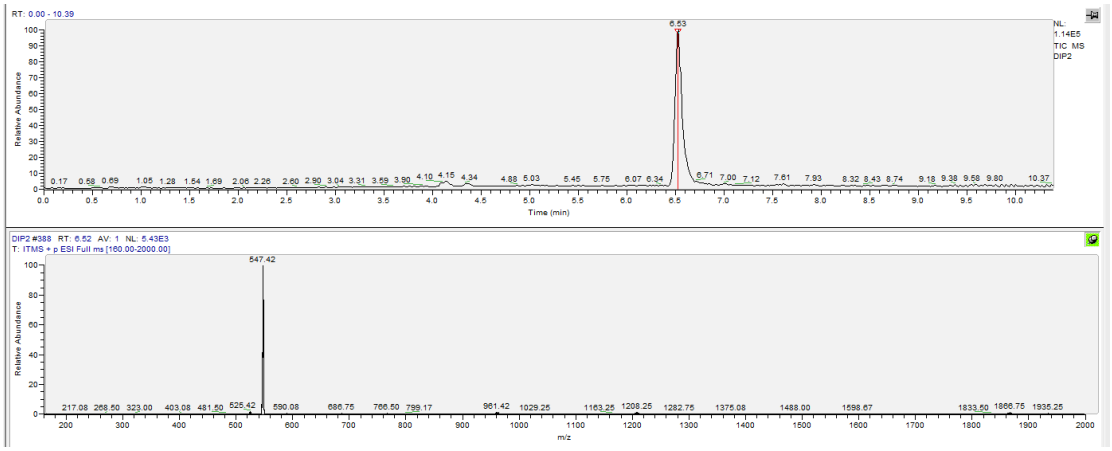

Figure S32 *LC-MS chromatogram of* ***Ru-DIP-O4*****.**

DLS analysis – aggregation studies

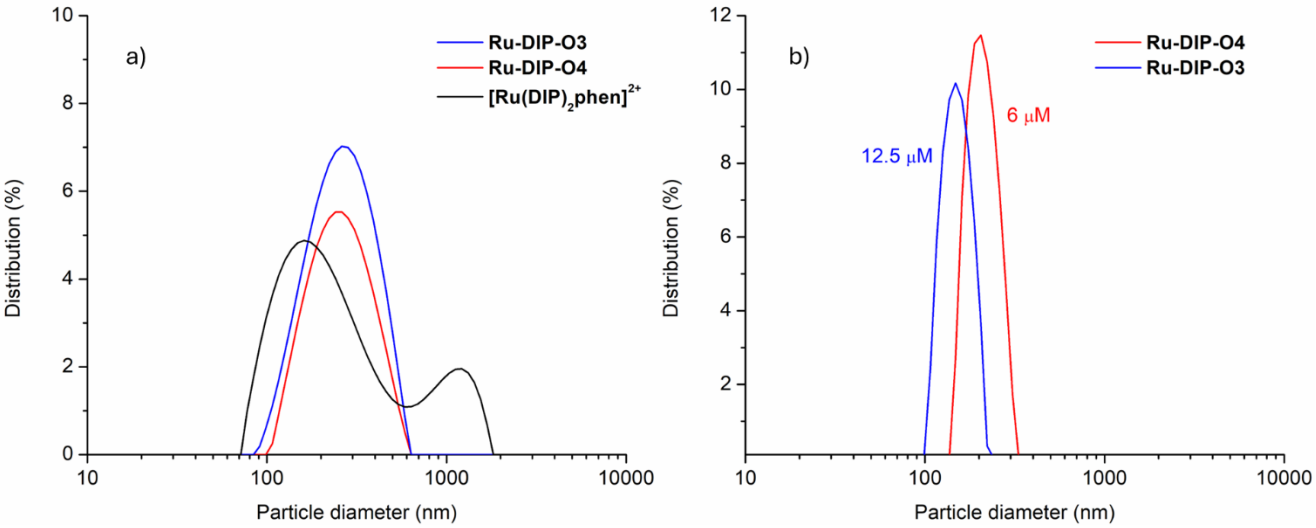

Figure S33 *DLS analysis results.* ***a)*** *Particle size distributions of relevant compounds in M9 bacteria growth medium.* ***b)*** *Particle size distributions of relevant complexes in the lowest concentrations where aggregation is evident with DLS analysis in Tris-HCl buffer.*

Compound	***Tris-HCl buffer***				***M9 media***			
	Hydrodynamic diameter (nm)		**Polydispersity index**		**Hydrodynamic diameter (nm)**		**Polydispersity index**	
	Average	St. dev.	Average	St. dev.	Average	St. dev.	Average	St. dev.
Ru-DIP-O3	259	14.7	18.1	5.44	271	78.1	25.1	1.6
Ru-DIP-O4	287	4.1	11.7	3.52	341	8.1	20.1	4.6
[Ru(DIP)$_2$phen]$^{2+}$	416	134	32.4	7.25	605	224	28.7	4.3

Table S1 *DLS analysis data.*

Photophysical studies

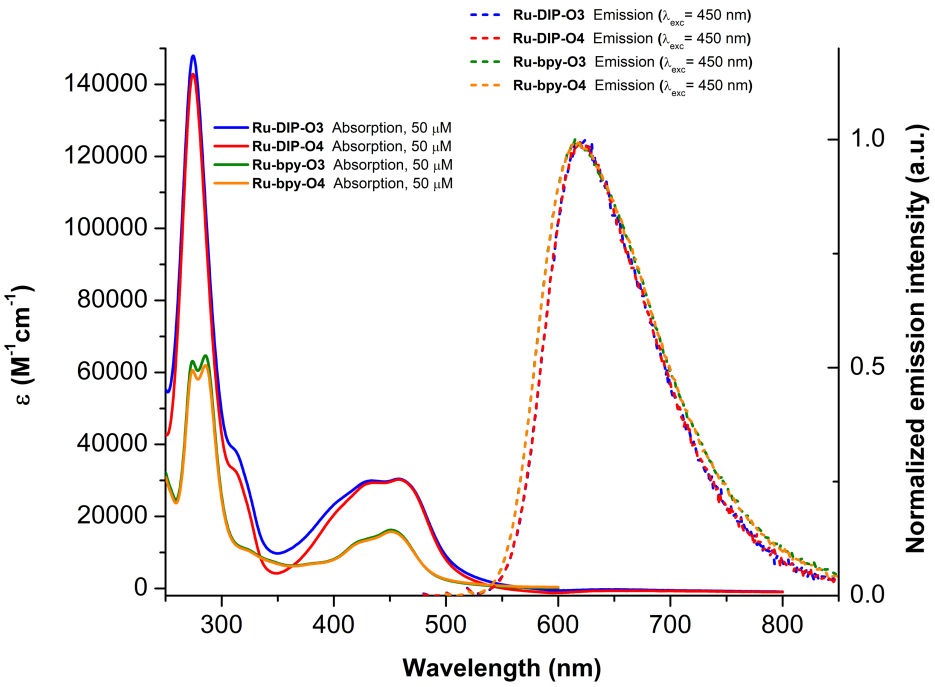

Figure S34 *Absorption (solid lines) and emission (dashed lines) profiles of all compounds in MeCN.*

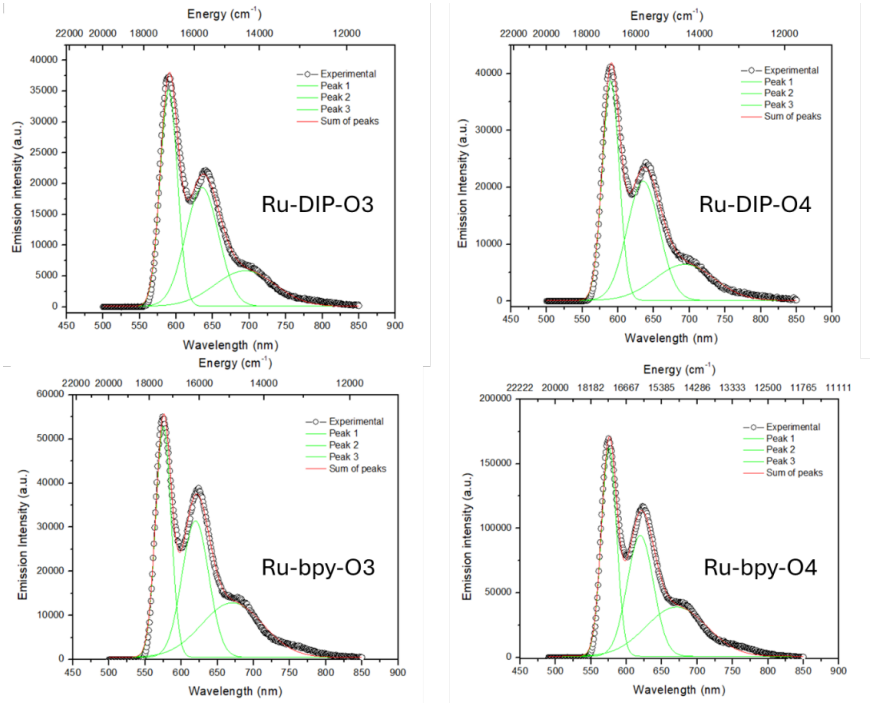

Figure S35 *Emission spectra of all complexes in 77 K glass matrix (λ_{exc} = 450 nm) along with their deconvolutions using Gaussian functions.*

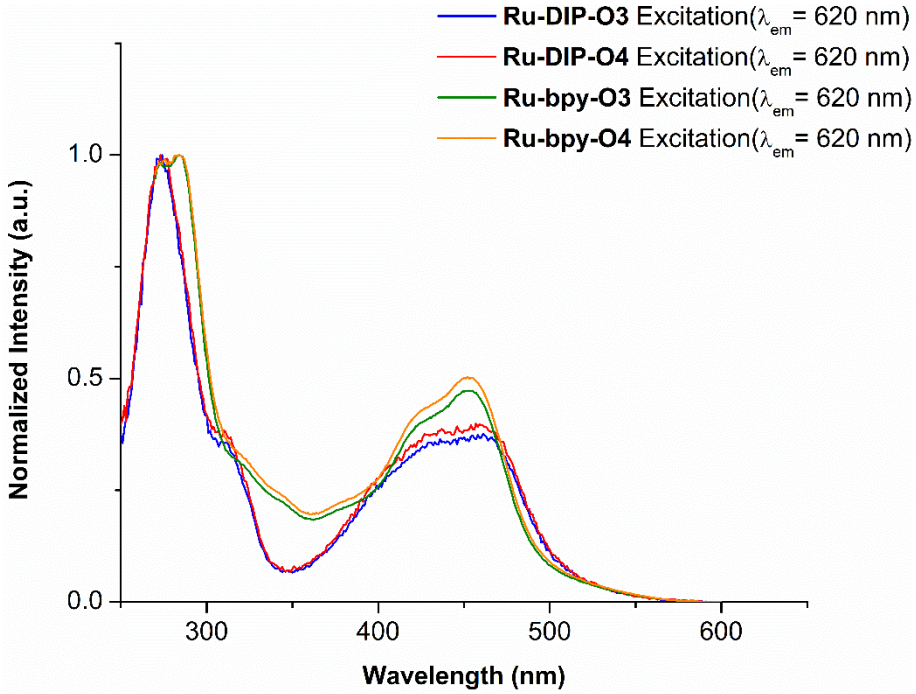

Figure S36 *Normalized excitation spectra of all compounds in Tris-HCl buffer (0.05 M, pH = 7.4) monitored at 620 nm.*

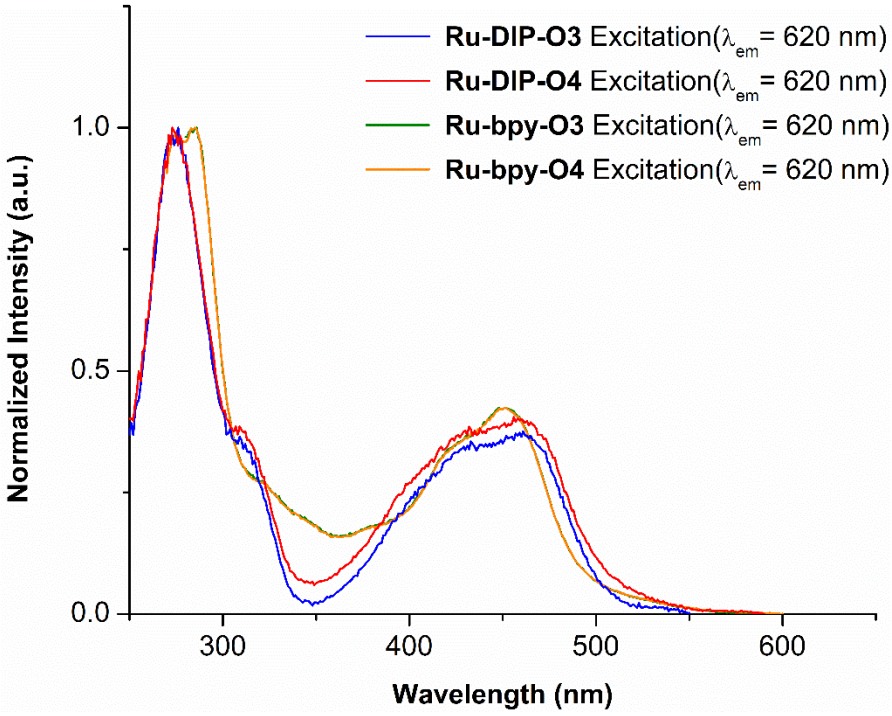

Figure S37 *Normalized excitation spectra of all compounds in MeCN monitored at 620 nm.*

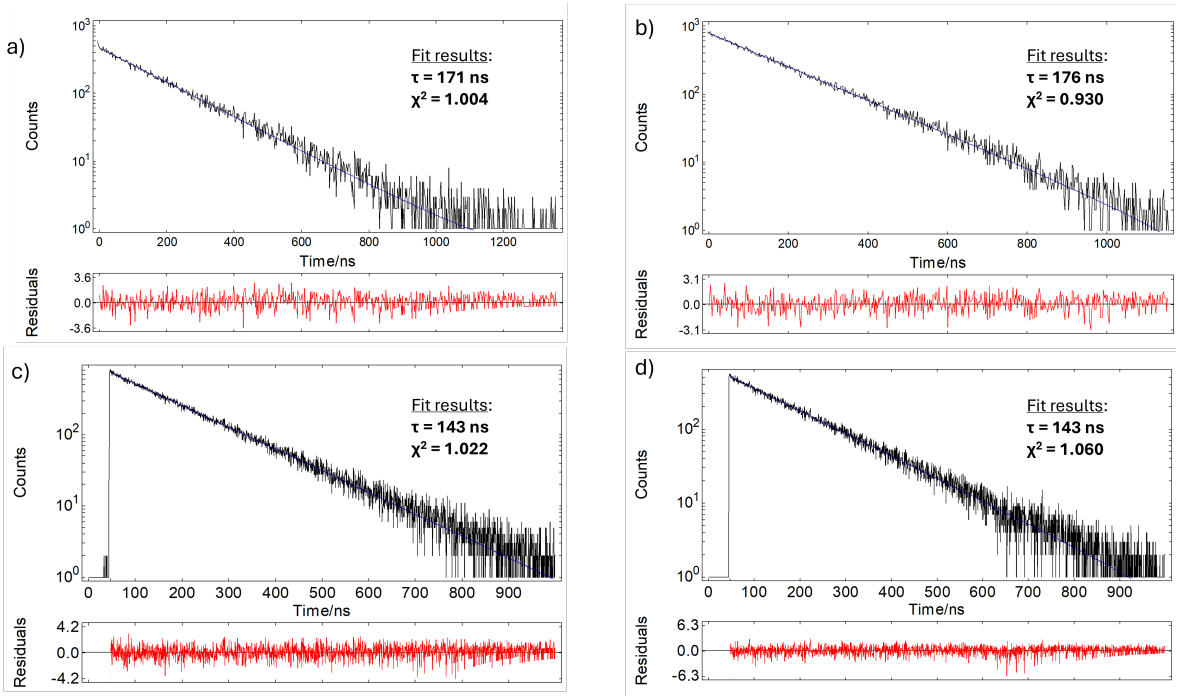

Figure S38 Experimental luminescence decay data and exponential fittings in MeCN for a) **Ru-DIP-O3**, b) **Ru-DIP-O4**, c) **Ru-bpy-O3**, d) **Ru-bpy-O4**.

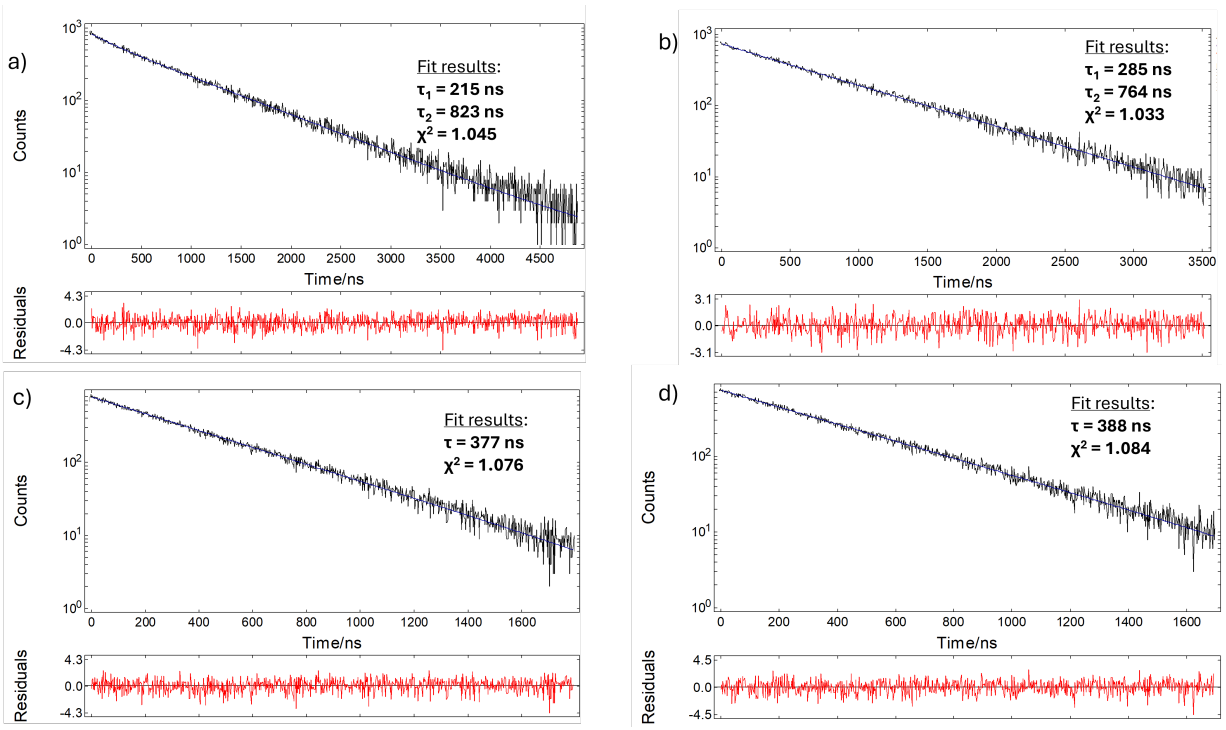

Figure S39 *Experimental luminescence decay kinetics (black) and exponential fittings (blue) in Tris-HCl buffer (0.05 M, pH = 7.4) for a)* ***Ru-DIP-O3****, b)* ***Ru-DIP-O4****, c)* ***Ru-bpy-O3****, d)* ***Ru-bpy-O4****.*

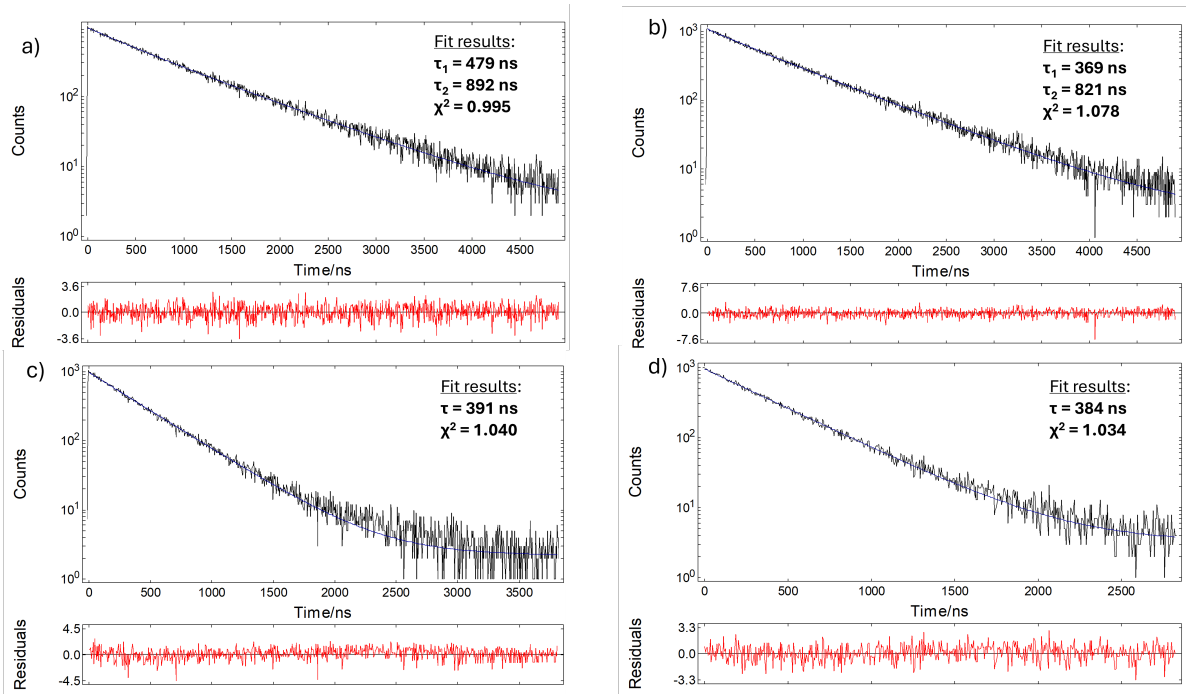

Figure S40 *Experimental luminescence decay kinetics (black) and exponential fittings (blue) in M9 buffer for a)* ***Ru-DIP-O3****, b)* ***Ru-DIP-O4****, c)* ***Ru-bpy-O3****, d)* ***Ru-bpy-O4****.*

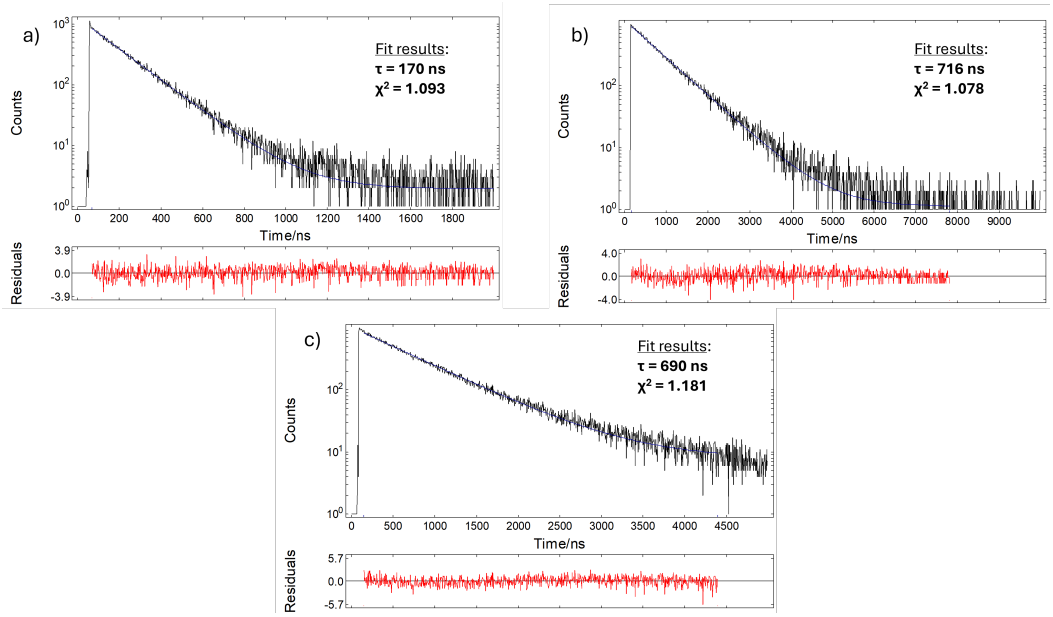

Figure S41 *Experimental luminescence decay kinetics (black) and exponential fittings (blue) of* $[Ru(DIP)_2phen]^{2+}$ *in a) MeCN, b) Tris-HCl buffer and c) M9 buffer*

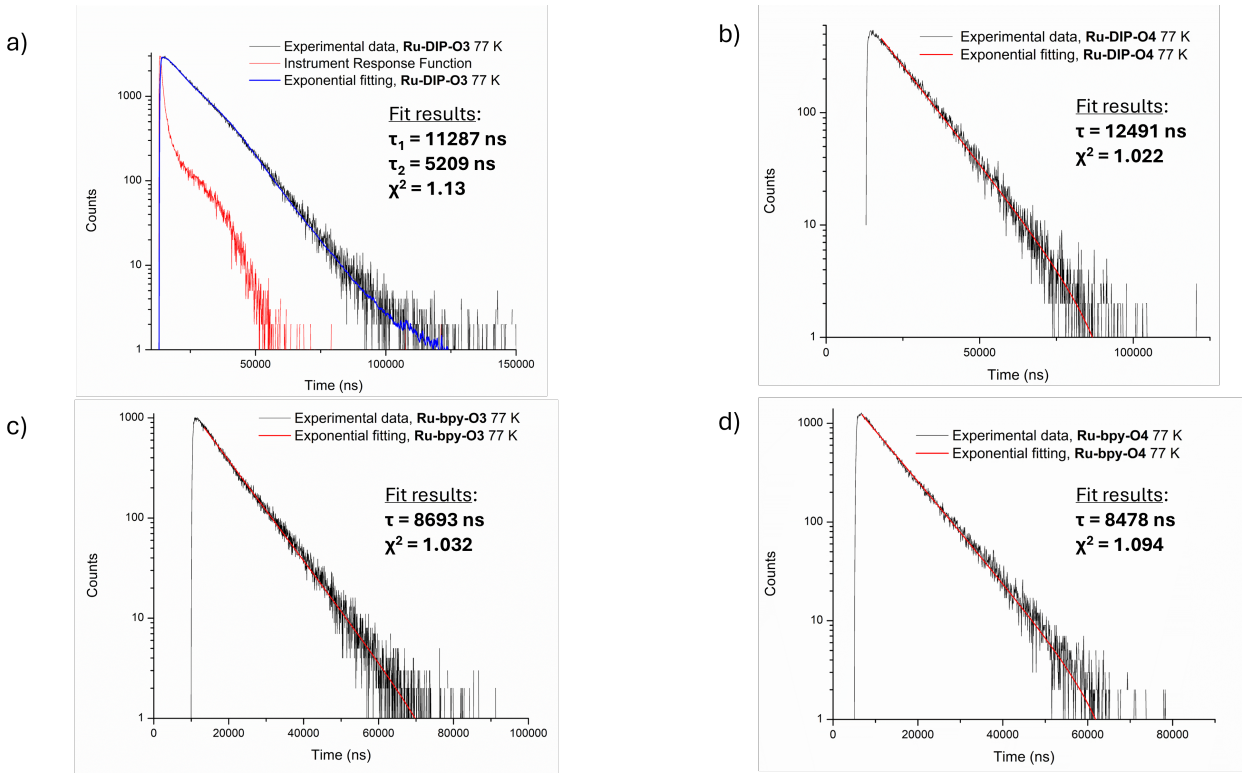

Figure S42 *Emission lifetime measurements for all complexes at 77 K in ethanol/methanol (4:1) frozen glass matrix.*

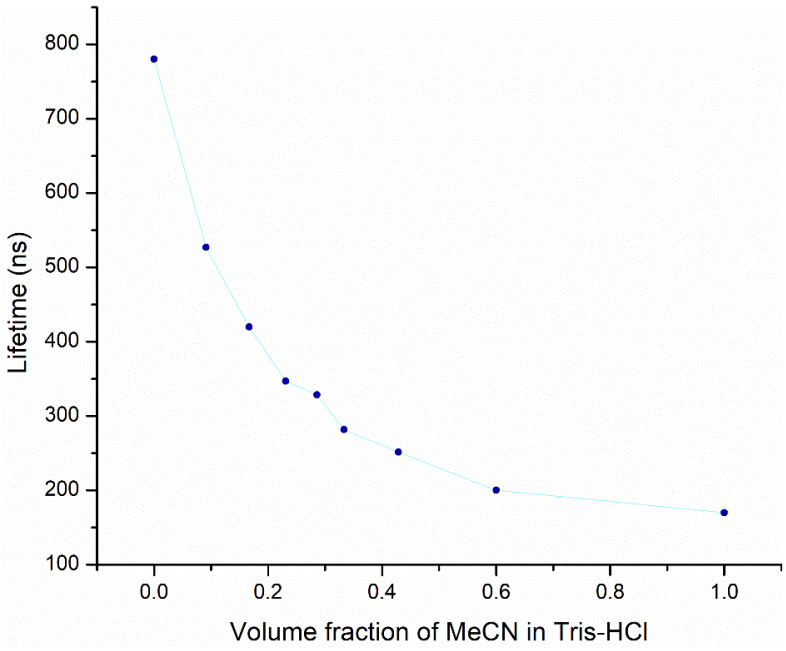

Figure S43 *Emission lifetimes upon gradually increasing MeCN volume fraction in Tris-HCl buffer (0.05 M, pH = 7.4) for* ***Ru-DIP-O4****.*

ROS generation studies

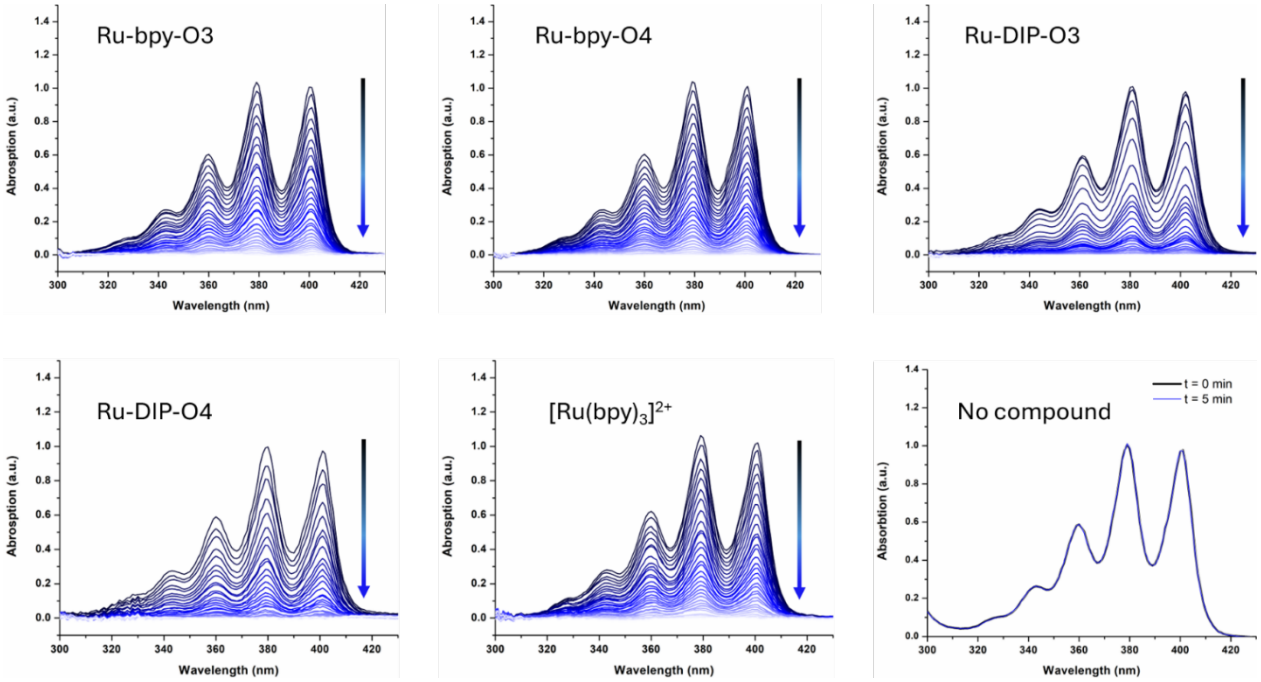

Figure S44 *ABDA assay results for all compounds. Endoperoxidation of the ABDA dye, due to photogeneration of $^1O_2$ is evident by the drop in absorption.*

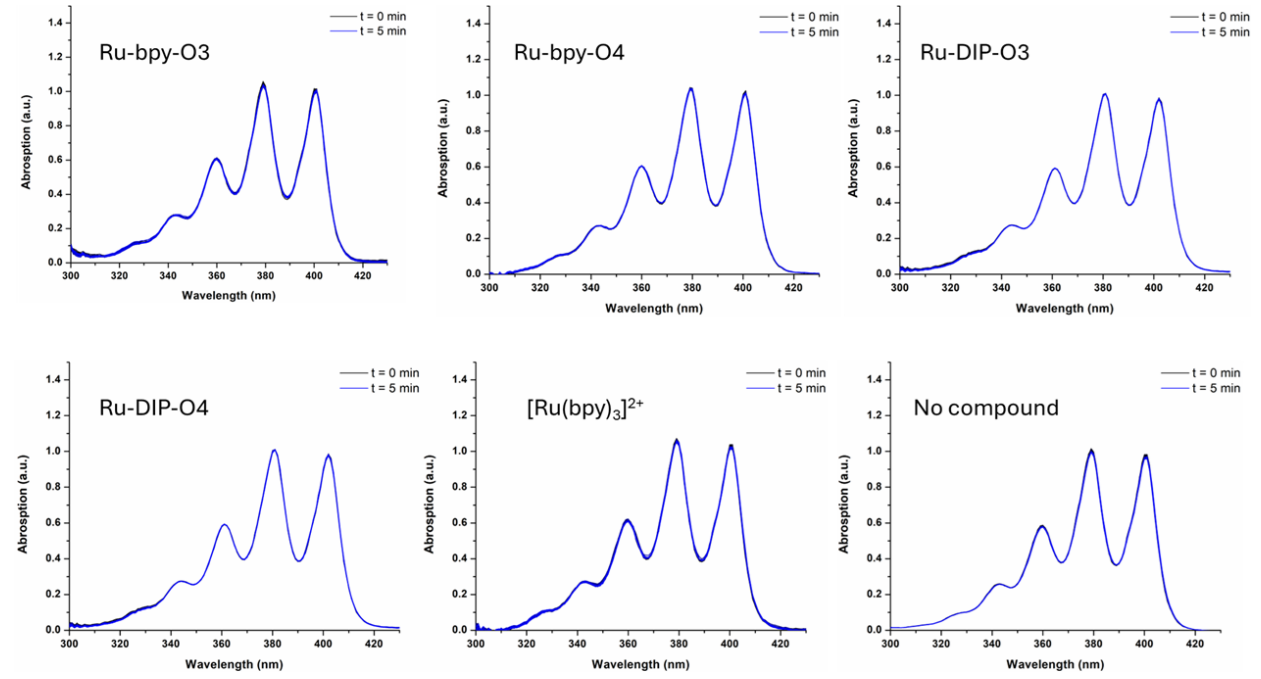

Figure S45 *ABDA assay results for all compounds without irradiation. No endoperoxidation is evident.*

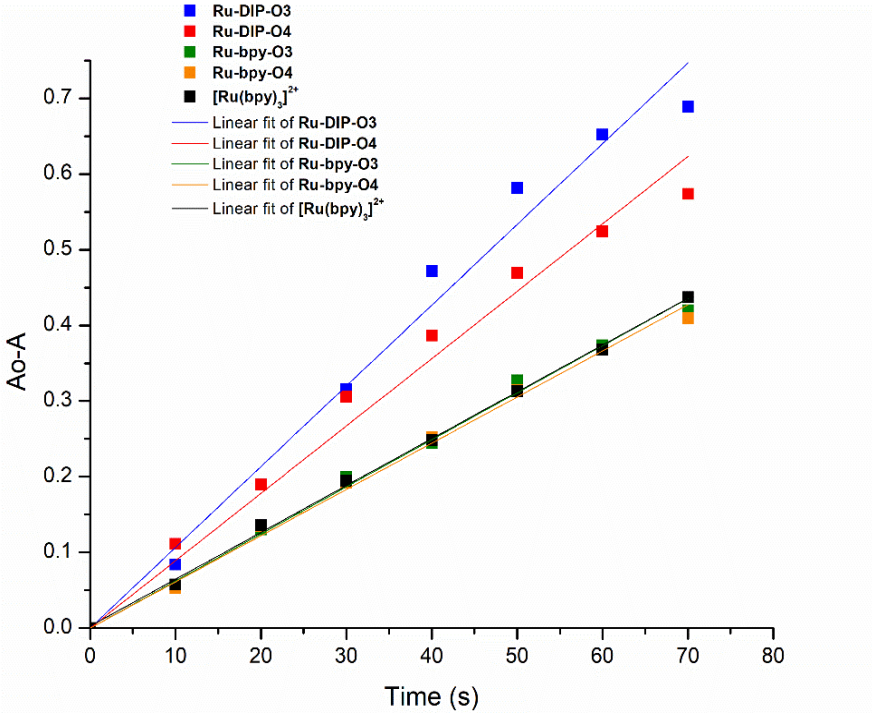

Figure S46 *Linear fittings of ABDA assays for all compounds.*

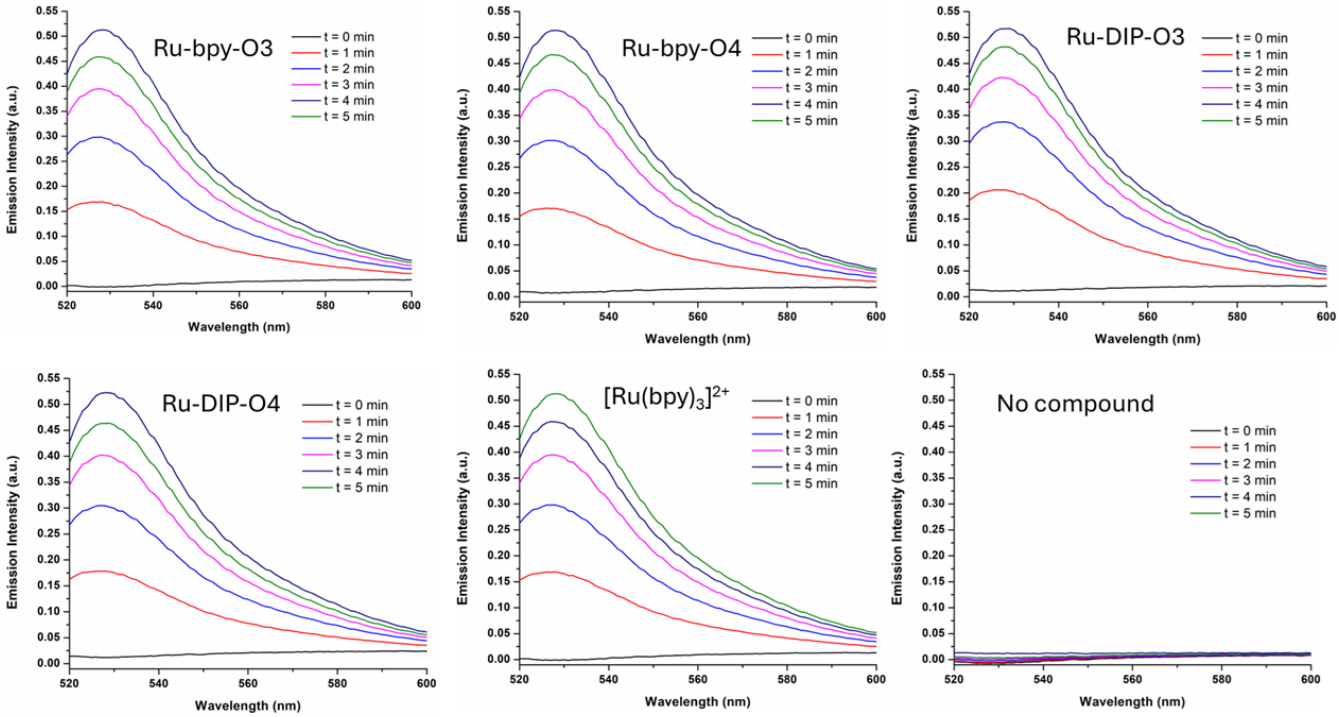

Figure S47 *DHR-123 assay results for all compounds. Conversion of the dye to its fluorescent derivative by photogenerated ROS is evident by the increase in emission.*

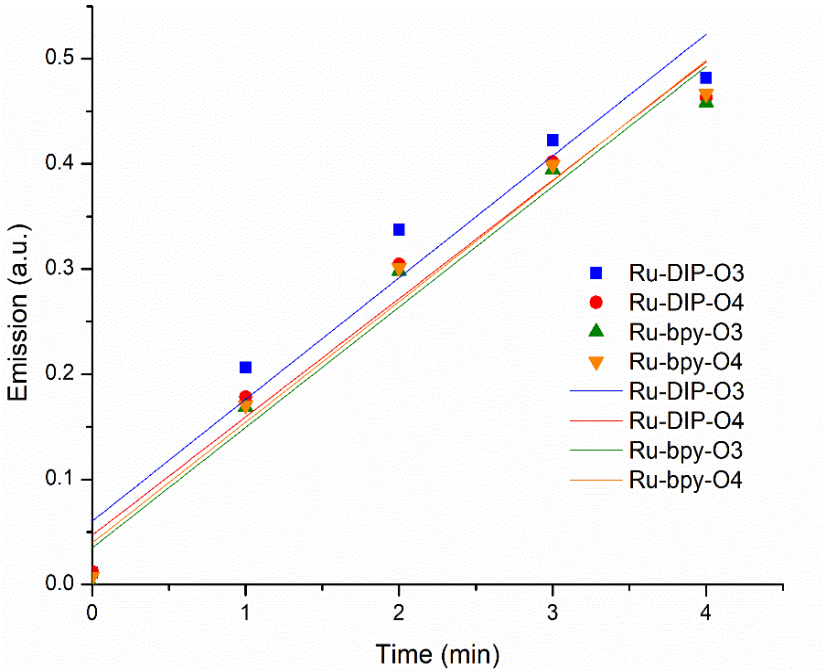

Figure S48 *Linear fittings of DHR-123 assays for all compounds.*

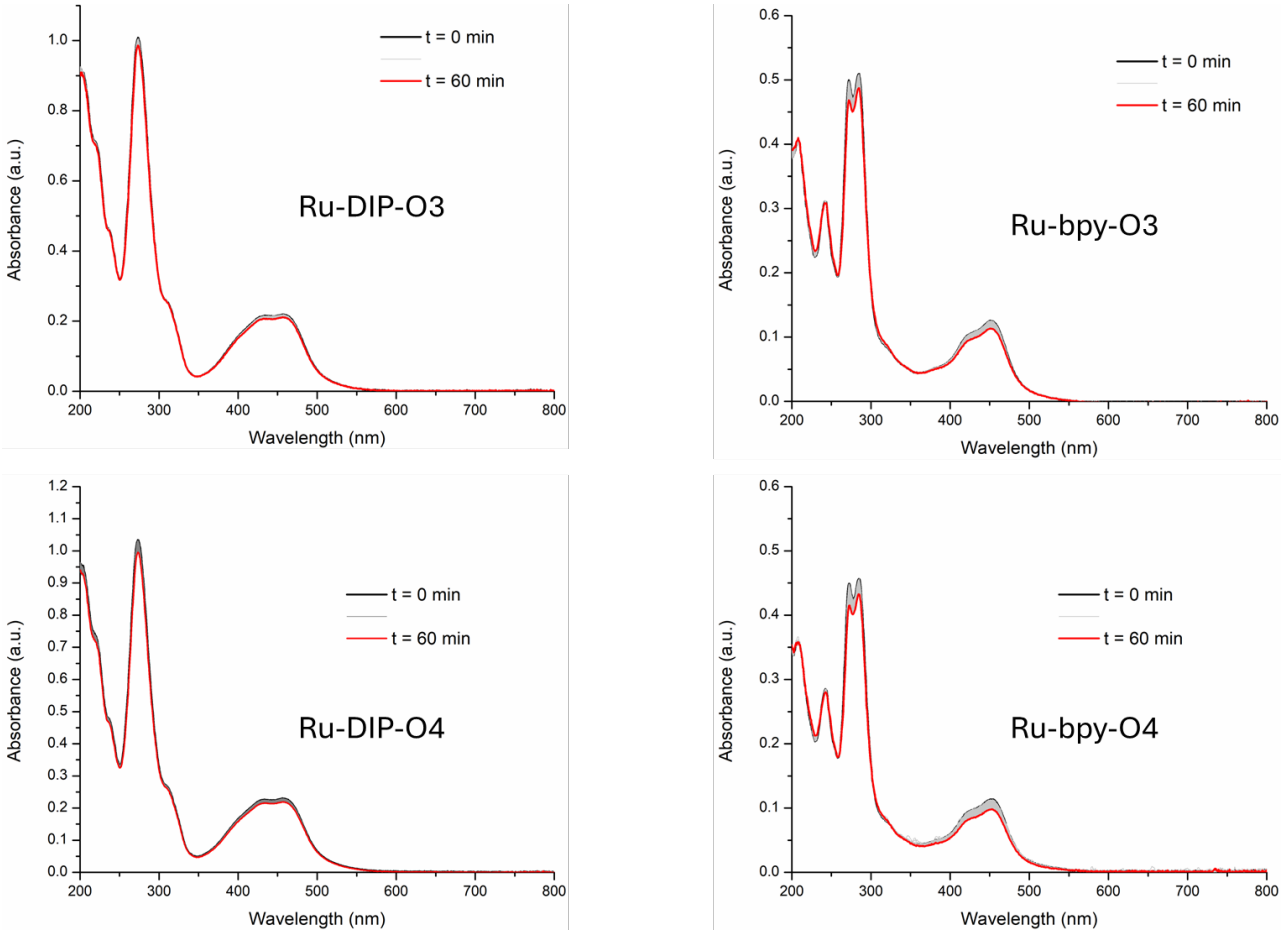

Figure S49 *Photostability assessment for all compounds. Continuous irradiation (450 nm) for 1 hour, no significant distortion in the absorption profile from t = 0 (black line) to t = 60 min (red line).*

Antibacterial SEM studies

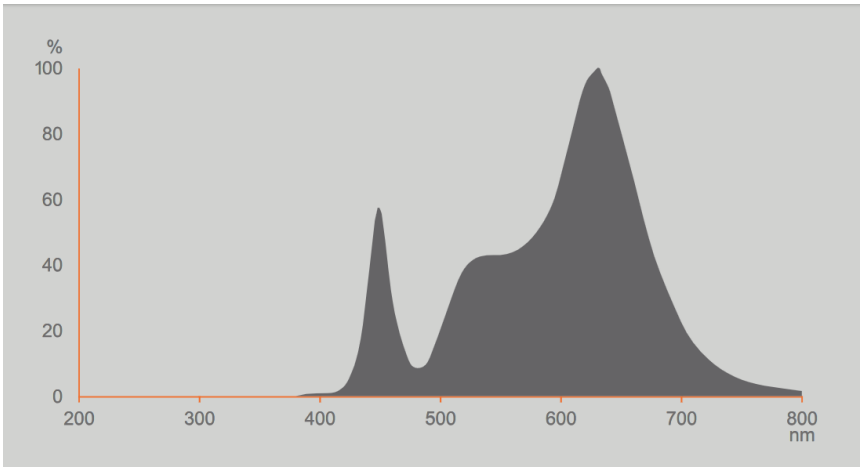

Figure S50 *Emission spectrum of fluorescent lamps used for antibacterial studies.*

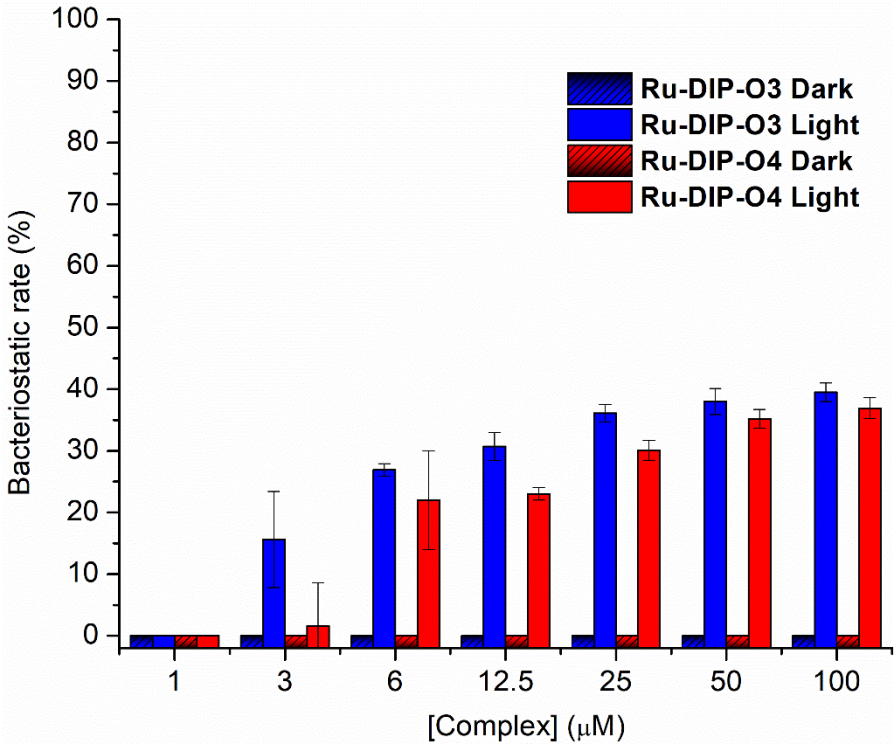

Figure S51 *In vitro antibacterial activity of* ***Ru-DIP-O3*** *and* ***Ru-DIP-O4*** *against E. coli in different concentrations*

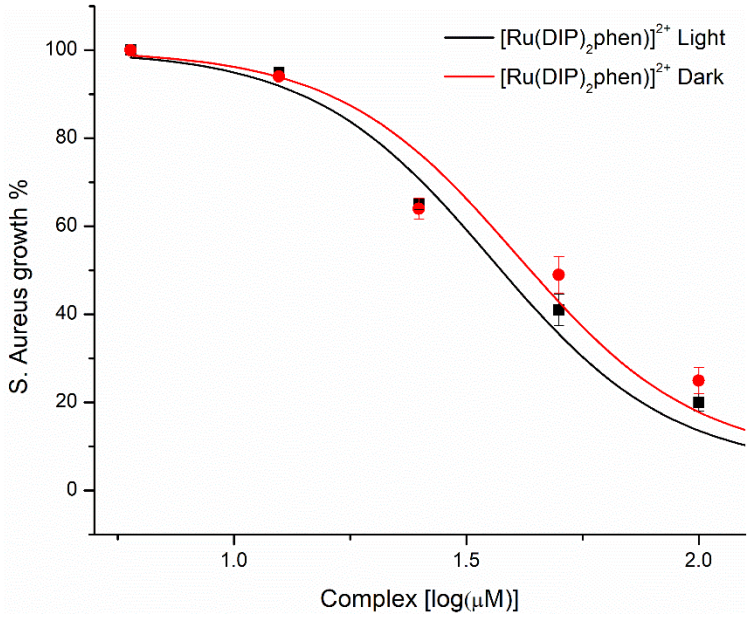

Figure S52 *Dose response fittings for* ***[Ru(DIP)₂phen]²⁺*** *activity against S. Aureus upon irradiation (black) and in dark condition (red).*

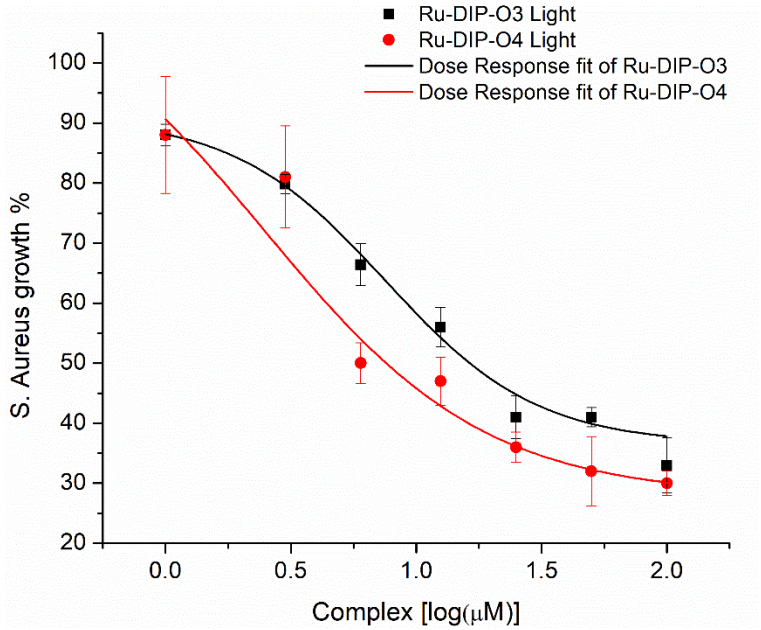

Figure S53 *Dose response fittings for* ***Ru-DIP-O3*** *(black) and* ***Ru-DIP-O4*** *(red) activity against S. Aureus upon irradiation.*

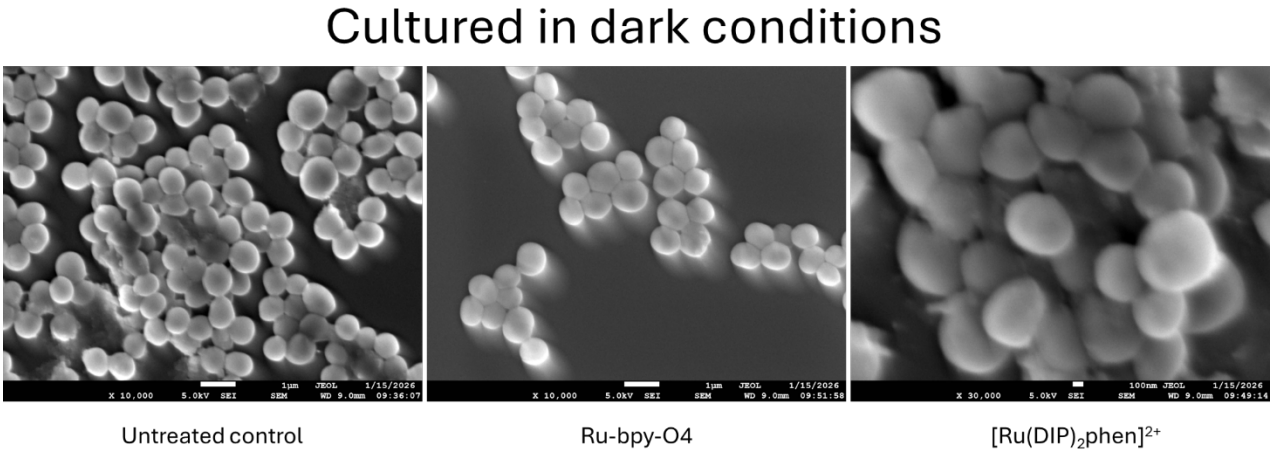

Figure S54 *SEM images of S. aureus treated with control compounds in dark conditions (for comparison with active compound in main text).*

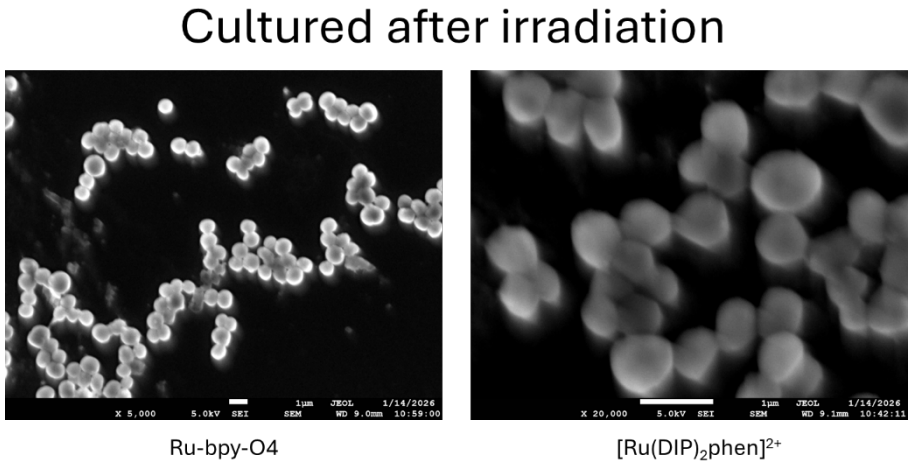

Figure S55 *SEM images of S. aureus treated with control compounds and subsequent irradiation (for comparison with active compound in main text).*